

# CO<sub>2</sub> and hydrography acquired by Autonomous Surface Vehicles from the Atlantic Ocean to the Mediterranean Sea: data correction and validation

Riccardo Martellucci<sup>1</sup>, Michele Giani<sup>1</sup>, Elena Mauri<sup>1</sup>, Laurent Coppola<sup>2</sup>, Melf Paulsen<sup>3</sup>, Marine Fourier<sup>2</sup>, Sara Pensieri<sup>4</sup>, Vanessa Cardin<sup>1</sup>, Carlotta Denticio<sup>5</sup>, Roberto Bozzano<sup>4</sup>, Carolina Cantoni<sup>6</sup>, Anna Luchetta<sup>6</sup>, Alfredo Izquierdo<sup>7</sup>, Miguel Bruno<sup>7</sup>, and Ingunn Skjelvan<sup>8</sup>

<sup>1</sup>National Institute of Oceanography and Applied Geophysics (OGS), Trieste, Italy

<sup>2</sup>Oceanography Laboratory of Villefranche (LOV), Villefranche, France

<sup>3</sup>GEOMAR Helmholtz Centre for Ocean Research Kiel, Kiel, Germany

<sup>4</sup>National Research Council - Institute for the study of Anthropic Impact and Sustainability in the Marine Environment (CNR-IAS), Genova, Italy

<sup>5</sup>Department of Environmental Sciences, Informatics and Statistics, Università Cà Foscari, Venice, Italy

<sup>6</sup>National Research Council-Institute of Marine Sciences (CNR-ISMAR), Trieste, Italy

<sup>7</sup>University of Cádiz (UCA), Spain

<sup>8</sup>NORCE Norwegian Research Centre, Bjerknes Centre for Climate Research. Bergen, Norway

Corresponding author: Riccardo Martellucci (rmartellucci@ogs.it)

**Abstract.** The ATL2MED demonstration experiment involved two autonomous surface vehicles from Saildrone Inc. (SD) which travelled a route from the eastern tropical North Atlantic to the Adriatic Sea between October 2019 and July 2020. This nine-month experiment in a transition zone between the temperate and tropical belts represents a major challenge for SD's operations. **The sensors on board were exposed to varying degrees of degradation and biofouling depending on the geographical area and season, which led to a deterioration of the measurements.** As a result, **some** maintenance measures were required during the mission.

We address the difficulty of correcting the data during a period of COVID-19 restrictions, which significantly reduced the number of discrete samples planned for SD salinity and dissolved oxygen validation. This article details alternative correction methods for salinity and dissolved oxygen. Due to the lack of *in situ* data, model products have been used to correct the salinity data acquired by the SDs, and then the resulting corrected salinity was validated with data from fixed ocean stations, gliders, and Argo floats. In addition, dissolved oxygen data acquired from SDs after correction using air oxygen measurements were tested and found to be coherent with the variation of oxygen concentrations expected from change in temperature and phytoplankton abundance (from chlorophyll-a). The correction methods are relevant and useful in situations where validation capabilities are lacking, which was the case during the ATL2MED demonstration experiment. **For future experiments, a more frequent sample collection would improve the data qualification and validation.**

## 1 Introduction

Automated observations contribute to a steadily increasing knowledge of the ocean and its role in the global climate system. For a long time, fixed ocean stations and research vessels formed the backbone of the monitoring network. In recent years, efforts have been made to improve the frequency of acquisition through technological developments (e.g., EU infrastructures ICOS, <https://www.icos-cp.eu/>; EMSO, <https://emso.eu/>; EuroArgo,

41 <https://www.euro-argo.eu>). Among other improvements, fixed ocean stations and ships of opportunity (Lüger et al., 2004) were equipped with autonomous and accurate sensors for partial pressure of CO<sub>2</sub> ( $p\text{CO}_2$ ) measurements in addition to sensors for complementary measurements (e.g., water temperature, salinity, dissolved oxygen, pH, nutrients, fluorescence) needed to understand the dynamics and the effects of CO<sub>2</sub> fluxes on the carbon budget. Despite efforts to do so, it remains difficult to obtain a comprehensive overview of CO<sub>2</sub> fluxes at regional and larger scales because of very sparse coverage by fixed observatories, low measurement frequency and limited systematic reference measurements.

48 One way to address such observational gaps (Tanhua et al., 2019) is to develop and deploy Autonomous Surface Vehicles (ASV) equipped with a suite of sensors, and capable of measuring CO<sub>2</sub> fluxes at the air-sea interface with gas reference, high sampling frequency and real-time data transmission. ASV monitoring systems have the potential to collect data from large ocean areas and at a frequency that resolves processes at multiple time scales. Nevertheless, there are challenges with those surface monitoring systems, and one of the most important is the biofouling, which can interfere with measurements of e.g., conductivity, dissolved oxygen and especially chlorophyll-a (Chl-a), and could ultimately render the sensors inoperable (e.g., Delauney et al., 2010). Regular maintenance counteracts biofouling or at least reduces the impact on measurements, but this is not always possible due to long distance from shore or from the maintenance vessel. Therefore, the value of ASV data depends heavily on quality control and quality assurance.

58 During the 9-month-long demonstration experiment ATL2MED, two wind-driven Sailsdrone ASV (SD; Gentemann et al., 2020) manufactured by Sailsdrone Inc. (Alameda, CA, USA) were used to improve data coverage and link CO<sub>2</sub> surface observations at fixed ocean stations on a larger scale from the eastern tropical North Atlantic (ETNA) to the central Mediterranean Sea. SDs are prone to errors primarily due to sensor drift, which can be caused by either biofouling or malfunctioning sensor parts. During the ATL2MED demonstration experiment, problems were found with the data collected by several SD sensors, and severe biofouling occurred, as expected in such a long-duration experiment.

65 Still, the use of SDs provided the opportunity to expand and link fixed CO<sub>2</sub> observations at the surface on a larger scale, particularly during the COVID-19 pandemic when access to ocean platforms and ship visits were restricted or even prohibited. Furthermore, the demonstration experiment allowed us to focus SD measurements on different marine environments, the Atlantic Ocean and the Mediterranean Sea, which made it possible to assess the quality of measurements across a wide range of values. The experiment additionally evaluated the ability of such ASV to provide data with sufficient quality to be relevant for the scientific community.

71 The objective of the present work is to evaluate and correct the data collected by the SDs in order to provide a homogenised and comparable data set useful for the study of processes such as air-sea gas exchange in the Atlantic Ocean and Mediterranean Sea. While this paper focuses on the methods, a follow up paper will focus on biogeochemical processes occurring in the area.

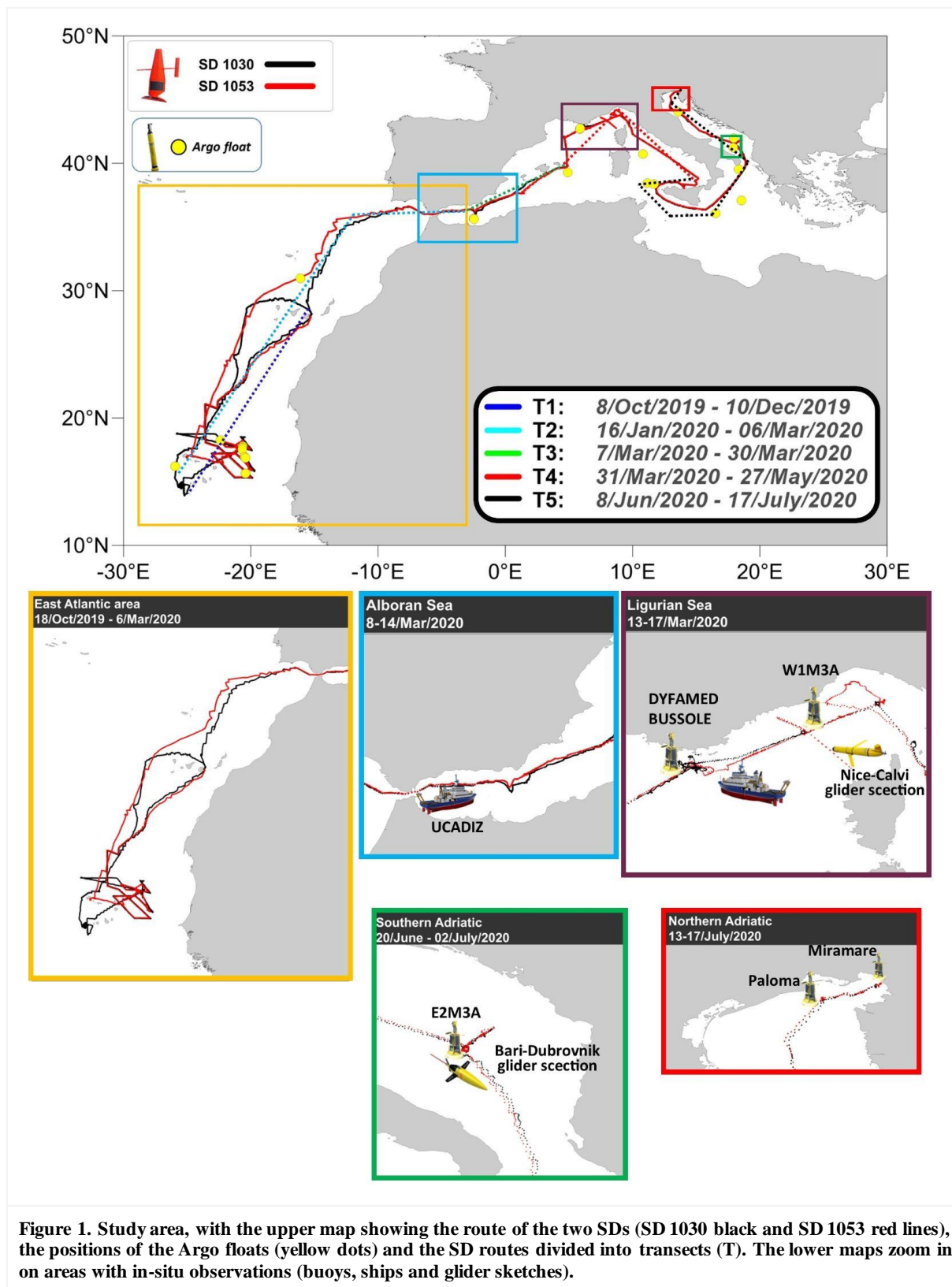
## 76 2 Material

### 77 2.1 Data collection and experiment

78 The ATL2MED demonstration experiment took place between 18 October 2019 and 17 July 2020 as a joint effort among a number of European academic institutions and SD piloting team. A detailed description of the ATL2MED demonstration experiment can be found in Skjelvan et al. (2021). During the experiment, the SDs crossed the ETNA region, the Strait of Gibraltar, and the northern part of the western and central Mediterranean Sea including the Ligurian Sea, the Strait of Sicily, the Strait of Otranto, and the Adriatic Sea (Fig. 1).

83 The aim of the ATL2MED demonstration experiment was to (1) study eddies in the Canary Current upwelling system off West Africa jointly with a vessel-based research expedition (RV Meteor M160) and (2) to validate the CO<sub>2</sub> measurements acquired at 5 fixed ocean stations (DYFAMED, W1M3A, E2M3A, PALOMA, and MIRAMARE). This monitoring experiment was achieved with sensors and instruments installed on the SDs, but also equipment deployed at a number of facilities that were used to correct data from the SDs (see Section 3). Table 1 provides an overview of the various facilities and the times at which the SD visits were carried out. A detailed description of the instruments and sensors installed on the different platforms as well as their characteristics can be found in Tables S1, S2 and S3 of the Supplementary Material.

91



92

93 Maintenance operations ensured the reliability and accuracy of the data collected by the SDs. Throughout the  
 94 expedition, the data collected by the SDs were categorised into different transects, designated as T1, T2, T3, T4,

95 and T5. These transects corresponded to specific sections of the expedition timeline in terms of maintenance events  
 96 (see Table S1 in Supplementary Material), which facilitates data correction.

97 The SDs were equipped with a number of autonomous sensors (CTD: conductivity, temperature, depth;  
 98 dissolved oxygen; fluorescence; pH;  $p\text{CO}_2$ ; meteorological sensors). **This study focuses primarily on sensors**  
 99 **acquiring temperature, salinity, dissolved oxygen, and  $p\text{CO}_2$  data.** This selection is based on the available options  
 100 for correcting the SD datasets: some of the sensors (*e.g.*, fluorescence) were so severely affected by biofouling  
 101 that it could not be accounted for, while others only worked for a short period of time (*e.g.*, DuraFet Honeywell  
 102 pH sensor). One of the SDs (SD 1030) was equipped with an ASVCO<sub>2</sub> system developed by PMEL (NOAA's  
 103 Pacific Marine Environmental Laboratory). The ASVCO<sub>2</sub> system is a compressed version of the more voluminous  
 104 system described in detail in Sutton et al. (2014). Water from a depth of approximately 0.5 m is fed into a bubble  
 105 equilibrator (Friederich et al., 1995) and the partially dried  $x\text{CO}_2$  is measured with an infrared detector (LI-COR  
 106 820 CO<sub>2</sub> gas analyser). A two points calibration was used where the first is a reference gas from NOAA/ERSL,  
 107 while the second is air purged for CO<sub>2</sub>. An air inlet was mounted approximately 1 m above sea level and  
 108 atmospheric  $x\text{CO}_2$  was measured between measurements of the sea surface. See Table S2 in the Supplementary  
 109 Material for the measurement frequency and initial accuracy of the SD sensors during the ATL2MED experiment.

110

## 111 2.2 Comparative datasets

### 112 2.2.1 Liguro-Provencal basin facilities

113 In the French EEZ, the open fixed station DYFAMED is located in the Ligurian Sea in the northwestern  
 114 Mediterranean Sea. The CNRS (French National Centre for Scientific Research) is in charge of the station as part  
 115 of the national MOOSE program (Coppola et al., 2019). At the DYFAMED site, a CARIOCA  $p\text{CO}_2$  sensor ensures  
 116 autonomous measurements and detailed description can be found in Merlivat et al. (2018). In addition, gliders are  
 117 regularly operating the Nice-Calvi section where the DYFAMED site is located (MOOSE program; Coppola et  
 118 al., 2019; Bosse et al., 2015; Testor et al., 2019). During the demonstration experiment, a deployment of the  
 119 Slocum glider was used along the endurance line (MOOSE T00-43 mission) performed from 12 March to 20 June  
 120 2020. Table S2 includes information about which sensors the glider was equipped with. Discrete samples were  
 121 collected from the DYFAMED site in February and March 2020 for comparison with the  $p\text{CO}_2$  sensor  
 122 measurements (Table S4).

123 The open fixed station W1M3A is located in the Italian EEZ of the Liguro-Provencal basin. Operated by  
 124 CNR-IAS, the W1M3A consists of a large spar buoy and a subsurface mooring positioned in the immediate  
 125 vicinity. A detailed description of the observatory can be found in Canepa et al. (2015) and some of this information  
 126 is found in Table S2. Discrete samples were collected from W1M3A in October 2020 (Table S4).

127

### 128 2.2.2 Adriatic Sea facilities

129 The fixed station E2M3A is situated in the open sea of the southern Adriatic Sea and is operated by OGS.  
 130 Information on this site is found in Bozzano et al. (2013) and Ravaioli et al. (2016). In the southern Adriatic, the  
 131 OGS also regularly operates an ocean glider at the Bari-Dubrovnik section (Mauri et al., 2016; Pirro et al., 2022;  
 132 Kokkini et al., 2019). During the AT2MED demonstration experiment, the glider transect was extended to include  
 133 the area of the E2M3A fixed station from 12 June to 2 July 2020. During the 20-day campaign 250 dives between  
 134 20 to 950 m profiles separated by 3-5 km and 4-6 hours were collected. Table S2 contains information about the  
 135 specific sensors mounted at the glider.

136 In the Gulf of Trieste in the northern Adriatic, the coastal stations PALOMA (operated by CNR-ISMAR) and  
 137 MIRAMARE (operated by OGS) are situated. Description of the PALOMA station is found in Ravaioli et al.  
 138 (2016) and Cantoni et al. (2012), while the MIRAMARE site is described in Ravaioli et al. (2016). See Table S2  
 139 for information about which sensors are used at the sites. By means of comparing the  $p\text{CO}_2$  sensor measurements  
 140 performed at the sites, discrete carbon samples were collected near PALOMA on 15 July 2020 and in the vicinity  
 141 of MIRAMARE on 17 July 2020 (Table S4).

142

## 143 2.3 Shipboard data

144 Discrete samples for Dissolved Inorganic Carbon (DIC) and TA were collected onboard the RV Meteor (M160)  
 145 during fall 2019 and analysed by GEOMAR. Discrete samples for DIC, TA, pH, and dissolved oxygen are  
 146 regularly collected next to the fixed ocean stations, however, this was not always possible during the ATL2MED  
 147 demonstration experiment due to COVID-19 pandemic restrictions. Table S4 gives an overview of the discrete  
 148 samples collected during the ATL2MED demonstration experiment and their sampling depth and analysing  
 149 methods.

150 In addition, salinity was measured continuously on board of the RV Ucadiz at a depth of 2.3 m between 5 and  
 151 6 March 2020, when the SD crossed the Gibraltar Strait. Table S2 contains information about the sensor used.

152  
 153 **Table 1. Research vessels and fixed ocean stations from which temperature, salinity and/or carbon measurements were**  
 154 **compared with those of the SDs.**

Research vessel/ fixed station	Position	Institution	SD 1030	SD 1053
RV Meteor	17.80°N 20.60°W	GEOMAR (DE)	30 November 2019	12 December 2019
RV Ucadiz	36.55°N 6.31°W - 36.09°N 5.36°W	UCA (ES)	5-6 March 2020	5-6 March 2020
DYFAMED	43.42°N 7.87°E	CNRS (FR)	28 April 2020	23 April 2020
W1M3A*	43.83°N 9.12°E	CNR-IAS (IT)	29 April-2 May 2020	28 April-2 May 2020
E2M3A*	41.57°N 18.08°E	OGS (IT)	29 June-2 July 2020	29 June-23 July 2020
PALOMA*	45.62°N 13.57°E	CNR-ISMAR (IT)	15 July 2020	15 July 2020
MIRAMARE*	45.70°N 13.71°E	OGS (IT)	17 July 2020	17 July 2020

155 \* These stations are part of the ICOS station network (Steinhoff et al., 2019).  
 156

## 157 2.4 Argo Float

158 Float data were retrieved from the Argo Coriolis Global Data Assembly Center in France (GDAC;  
 159 <ftp://ftp.ifremer.fr/argo>, Wong et al., 2020). For each Argo float the variable SALINITY ADJUSTED was  
 160 extracted, and then used for comparison with SD salinity data. Every profile close in space and time (1 day and 30  
 161 km) was chosen and then salinity was averaged in the upper 5 m of the water column.  
 162

## 163 2.5 Model output

164 The Copernicus Marine Service (CMEMS) model product, specifically the Global Ocean 1/12° Physics Analysis  
 165 and Forecast (<https://doi.org/10.48670/moi-00016>) and the Mediterranean Sea Physics Analysis and Forecast  
 166 (Escudier et al., 2020, Clementi et al., 2021) were used. Daily data were developed for the global ocean and  
 167 Mediterranean Sea.  
 168

## 169 2.6 Satellite product

170 To evaluate the ocean response, sea surface Chl-a (OCEANCOLOUR\_MED\_BGC\_L3\_NRT\_009\_141), sea  
 171 surface temperature (Merchant et al., 2019, Buongiorno Nardelli et al., 2022) and the vertical structure of ocean



172 temperature (MEDSEA\_MULTIYEAR\_PHY\_006\_004) were downloaded from the CMEMS data portal and  
 173 analysed (Table S6 in the Supplementary Material).

174

## 175 3 Methods

### 176 3.1 Salinity

177 Here, the salinity is measured using the PSS-78 scale. During the first transect, T1 (Fig. 2), the two salinity sensors  
 178 on board the SDs showed high consistency (Fig. 2a, b). After the first maintenance in T2, the SD 1053 showed a  
 179 reduction in salinity of about 1 compared to the salinity measured by the SD 1030. In T3, the difference in salinity  
 180 decreased on average to 0.15. During this period, the SDs crossed the Alboran Sea characterised by high  
 181 thermohaline variability due to the presence of Atlantic and Mediterranean waters (Poulain et al., 2021), and the  
 182 high spatial and temporal variability in salinity distribution in the area (Capó et al., 2021) complicates the  
 183 understanding of the observed differences (i.e., sensor error or natural variability). In T4 and T5, salinity shifts of  
 184 1 were observed until the end of the experiment.

185 Given the large variability found in the salinity data of the SDs, a comparison with *in situ* data along the  
 186 trajectory of the experiment was necessary. We first identified the observing systems (fixed buoy, Argo float)  
 187 temporally and spatially close to the positions of the SDs. Salinity data, with a temporal and spatial interval lower  
 188 than 1 day and 30 km, respectively, were used for the comparison and/or correlation, however they were extremely  
 189 scarce.

190 To further evaluate the salinity data of the two SDs, a comparison was made with climatological data,  
 191 considering the closest point in the climatology dataset to the SDs measurements (Fig. 2). SD 1030 exhibited  
 192 consistent salinity data in periods T1, T2, and T4 ( $\Delta S < 0.1$ ), with deviations observed in periods T3 and T5 (Fig.  
 193 2a). Conversely, SD 1053 displayed consistent salinity data only in period T1 ( $\Delta S < 0.1$ ), with higher deviations in  
 194 periods T2, T3, T4, and T5. Subsequent evaluation of the data distribution characteristics revealed variances  
 195 between the two SDs (Fig. 2b).

196 In T5, the climatology failed to represent salinity in Ionian and Adriatic Sea, characterised by a continuous  
 197 increase in salinity since 2017 (Mauri et al., 2021; Mhianovic et al., 2021; Menna et al., 2022; Neri et al., 2023;  
 198 Pranic et al., 2023). This was due to the bipolar behaviour of the Ionian Sea, subject to an alternation between the  
 199 highly saline waters of the Levantine Basin and the less saline waters of Atlantic origin (Pinardi et al., 2019; Gacic  
 200 et al., 2021; Menna et al., 2022; Civitarese et al., 2023).

201 To overcome the problem of lack of data, we decided to compare the data acquired by the SDs with the  
 202 reanalysis model products along the entire route (Fig. 2a, b). The model, while not deviating much from the *in situ*  
 203 and climatological data (Fig. 2), can provide salinity products along the SD's trajectory allowing to correct the  
 204 salinity recorded by the SD. Moreover, comparative works between the physical model and experimental  
 205 observations have shown a satisfactory correlation both in the open ocean (Escudier et al., 2021; Menna et al.,  
 206 2023) and in the coastal environment (Martellucci et al., 2021). Despite any limitations a model may have in such  
 207 cases, the use of model products allows a minimum spatial and temporal distance in the comparison of the along  
 208 track SD measurements. **The nearest nodes (in km) with respect to the model data grid to the SD trajectory were**  
 209 **chosen.** The salinity provided by the model along the two SD trajectories shows very similar values to that  
 210 measured by SD 1030 (Fig. 3). Salinity differences between the CMEMS model and the SD 1030 observations  
 211 show a difference less than 0.1 in T1, T2, T4 and T5. During the Alboran Sea crossing (T3), the observed salinity  
 212 deviated strongly from the model (about 0.6) over only 20 days. In contrast, SD 1053 showed deviating values  
 213 compared to the model and SD 1030, which cannot be explained by space-time variability. With the exception of  
 214 T1, the remaining transects (Fig. 3i-j) showed large deviations between model and observed salinities (T2: 0.8,  
 215 T3: 0.7, T4: 0.9, and T5: 1). This could be related to the long time between the SD 1053 maintenance (early January  
 216 and early May 2020), but it is more likely that a sensor error occurred in mid-January which even maintenance  
 217 could not correct.

218 The salinity correction was performed using a linear regression method in which the salinity data recorded by  
 219 the autonomous vehicles averaged over the day, were calibrated with the corresponding data from numerical  
 220 models. A strict criterion, with a significance level of  $p < 0.05$  (Table 2), was applied to the correction process.

221

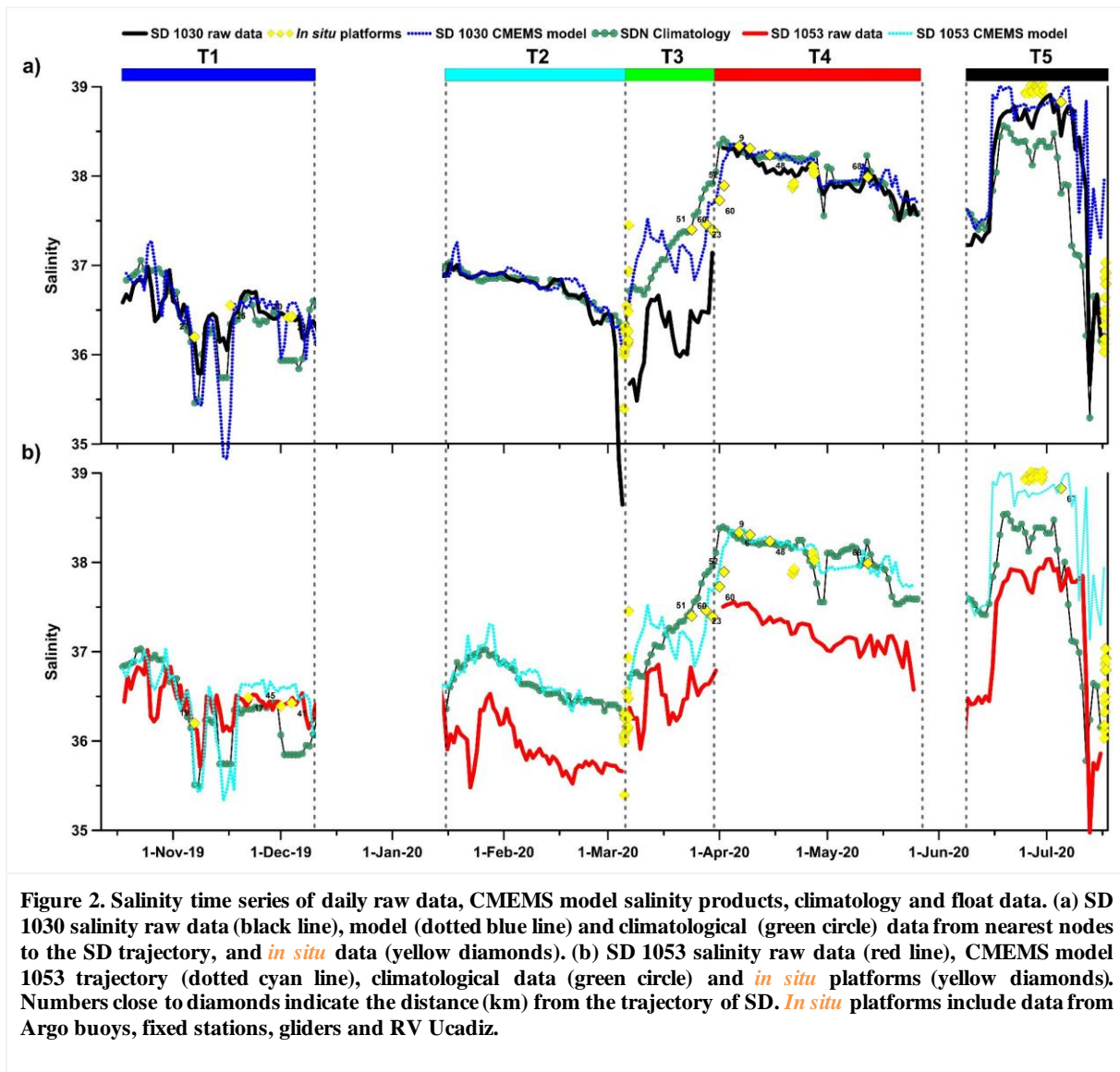


Figure 2. Salinity time series of daily raw data, CMEMS model salinity products, climatology and float data. (a) SD 1030 salinity raw data (black line), model (dotted blue line) and climatological (green circle) data from nearest nodes to the SD trajectory, and *in situ* data (yellow diamonds). (b) SD 1053 salinity raw data (red line), CMEMS model 1053 trajectory (dotted cyan line), climatological data (green circle) and *in situ* platforms (yellow diamonds). Numbers close to diamonds indicate the distance (km) from the trajectory of SD. *In situ* platforms include data from Argo buoys, fixed stations, gliders and RV Ucadiz.

222

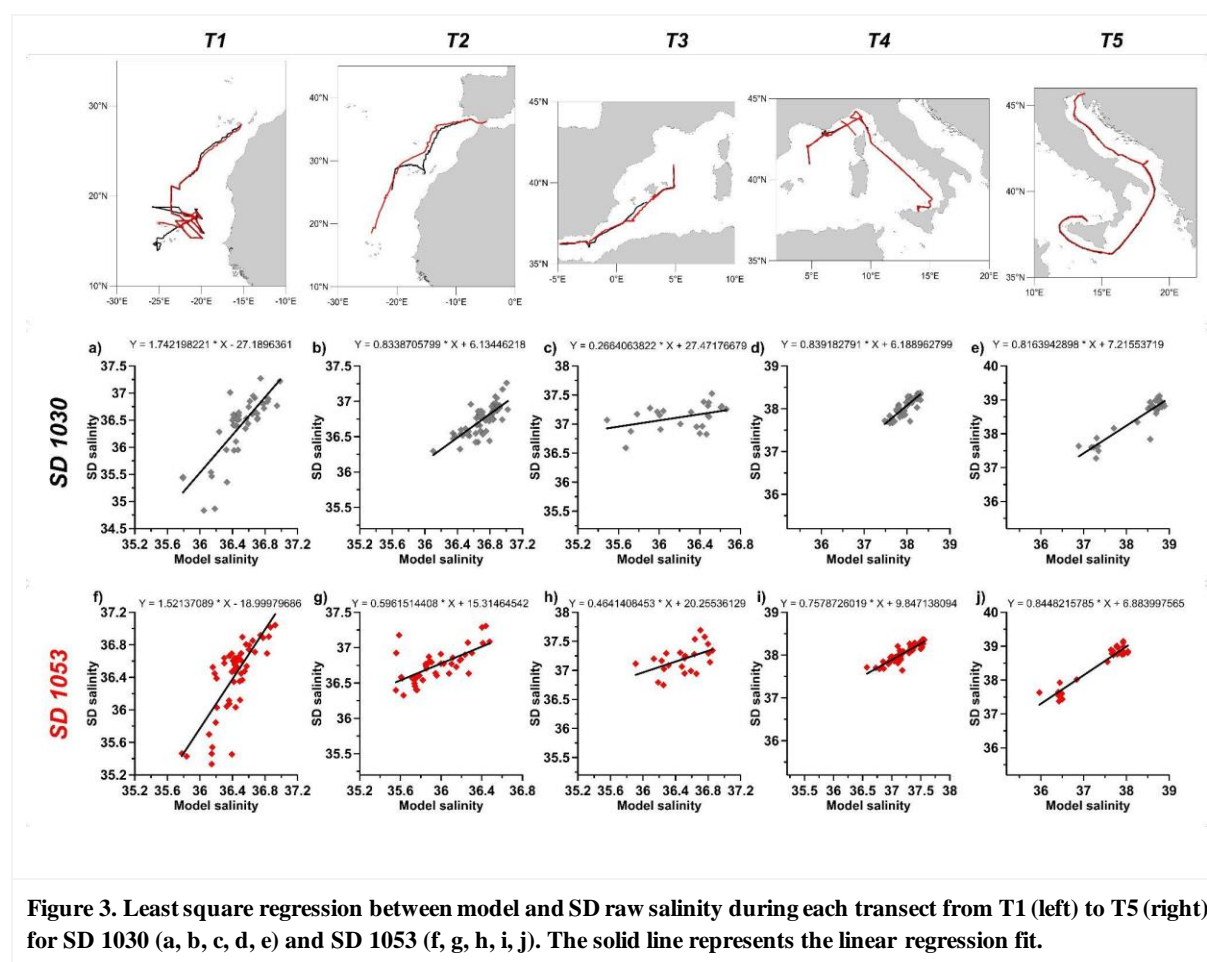
223 Table 2. Statistics for the salinity correction. T1, to T5 refer to the different transects, pval is the significance level,  
 224 distribution refers to normal or non normal data distribution,  $R^2$  is the correlation coefficient, RMSE is the root mean  
 225 square error, and NaN refers to lack of data.

		Direct comparison				
		<i>T1</i>	<i>T2</i>	<i>T3</i>	<i>T4</i>	<i>T5</i>
SD 1030	<i>pval</i>	0.0007	0.04	<0.001	0.04	0.025
	<i>distribution</i>	non normal	non normal	normal	non normal	normal
	<i>R2</i>	0.59	0.61	0.19	0.71	0.85
	<i>RMSE</i>	-	-	0.9058	-	0.2789

<b>SD 1053</b>	<i>pval</i>	0.026	0.003	0.004	<0.001	<0.001
	<i>distribution</i>	non normal	normal	normal	normal	normal
	<i>R2</i>	0.08	0.44	0.25	0.789	0.919
	<i>RMSE</i>	-	0.826	0.7072	0.8444	1.1275

226

227



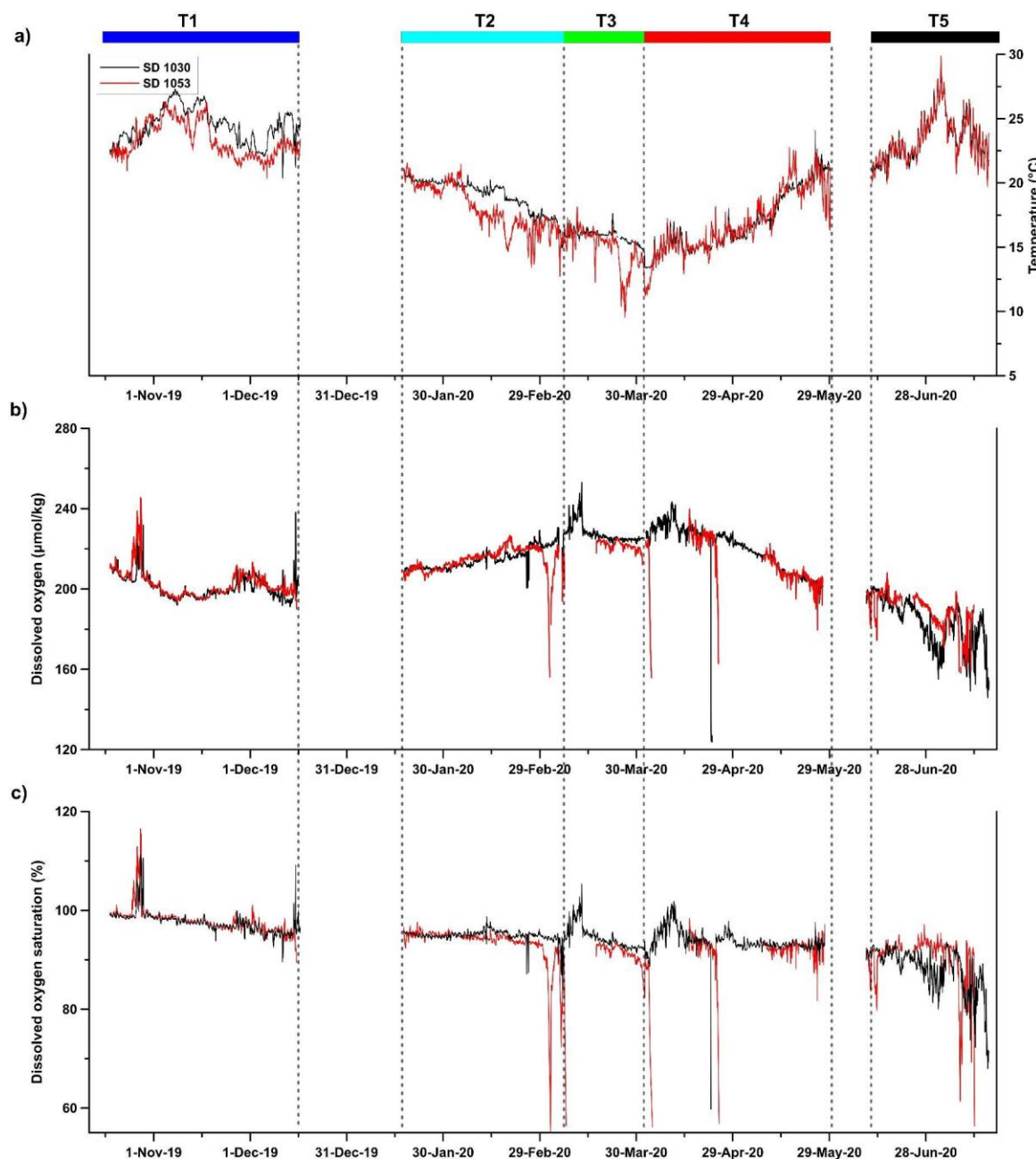
228

### 229 3.2 Dissolved Oxygen

230 Due to the strong dependence of dissolved oxygen on temperature, we first analyse the temperature along the track  
 231 of the SDs. During the demonstration experiment, sea temperature (Fig. 4a) showed a seasonal signal similar to  
 232 those observed at these latitudes (Pastor et al., 2019). The high observed temperature variability also includes the  
 233 wide geographical coverage of the SDs. The highest temperatures were measured in November 2019 and July  
 234 2020 in the tropical Atlantic and the southern Adriatic, respectively. The lowest temperatures were measured in  
 235 the Gulf of Lion in April 2020. Along the SD tracks, the salinity (Fig. 2b) showed a gradual increase from the  
 236 Atlantic Ocean to the eastern Mediterranean Sea. Given the correct temperature measurement, any dissolved  
 237 oxygen drift can be assessed through comparison with dissolved oxygen saturation values. This procedure was



238 also used to correct Argo float data with climatological observations (Takeshita et al., 2013). The dissolved oxygen  
 239 saturation showed a gradual decrease from 100% at the start of the demonstration experiment to 80% at the end  
 240 (Fig. 4c). This behaviour is also reflected in the dissolved oxygen concentration, which decreases by about 40  
 241  $\mu\text{mol/kg}$  for SD 1030 and 60  $\mu\text{mol/kg}$  for SD 1053 (Fig. 4b) over the course of nine months with standard deviation  
 242 of the uncorrected oxygen record of 16  $\mu\text{mol/kg}$  and 72  $\mu\text{mol/kg}$  for SDs 1030 and 1053, respectively.  
 243



244  
 245  
 246 **Figure 4. (a) Temperature, (b) dissolved oxygen concentration, and (c) dissolved oxygen saturation for the SD raw data**  
 247 **(SD 1030 black line and SD 1053 red line).**  
 248

249 Prior to applying correction all the outliers were excluded. After the first analysis we proceeded to correct the  
 250 dissolved oxygen data, using the same oxygen correction method as used in the Argo program (Bittig et al., 2018).  
 251 The principle of this method is to compare the dissolved oxygen measurements performed while the Argo oxygen  
 252 sensor is in air with the oxygen partial pressure ( $pO_2$ ) in air (Johnson et al., 2015). The latter variable is easily  
 253 calculated from air temperature, air pressure, and relative humidity acquired by the SDs. Considering that the SD  
 254 oxygen sensor is installed on the hull about 0.5 m below sea surface and that the SDs sailing cause mixing of the

255 water surface while sailing, we assume that the SDs oxygen sensors were in equilibrium with the atmosphere  
 256 above, and furthermore, we can correct for the oxygen sensor drift using the in air calibration method (Bittig et al.,  
 257 2018; Johnson et al., 2015). Specifically, we computed vapour pressure ( $V_p$ , in hPa) from the empirical equation  
 258 reported in the operating manual of Aanderaa oxygen optode (model4330) using the air temperature ( $T_{sd}$ ) recorded  
 259 from SDs:

$$260 \quad V_p = e^{(52.57 - (\frac{6690.90}{T_{sd} + 273.15})) - 4.681 \cdot \ln T_{sd} + 273.15} \quad (1)$$

261 and expected partial pressure ( $E_{pp}$ , in hPa) from volume fraction of oxygen ( $V_{fO_2}=0.20946$ ; Glueckauf, 1951),  
 262 atmospheric pressure ( $AP_{sd}$ ), vapour pressure ( $V_p$ ) and relative humidity ( $RH_{sd}$ ), as follows:

$$263 \quad E_{pp} = V_{fO_2} * (AP_{sd} - (V_p * \frac{RH_{sd}}{100})) \quad (2)$$

264 The  $E_{pp}$  was then compared to the  $pO_2$  from the SDs to compute the gain factor ( $G$ ) for daily correction.

$$265 \quad G = \frac{E_{pp}}{pO_{2sd}} \quad (3)$$

266 The corrected oxygen concentration ( $O_{2csd}$ ) from the SDs was calculated from adjusting the oxygen data from SDs  
 267 ( $O_{2sd}$ ) with the gain factor.

$$268 \quad O_{2csd} = G * O_{2sd} \quad (4)$$

269 For each transect the mean gain was calculated and then, the gain factor was multiplied by the hourly oxygen  
 270 data allowing to correct the time series.

271

## 272 3.3 Correction and adjustment of $pCO_2$ data

### 273 3.3.1 Fixed-sites $pCO_2$ data acquisition and qualification

274 The  $pCO_2$  measurements from the different fixed ocean stations were regularly compared to the  $pCO_2$  calculated  
 275 from discrete water samples collected by the fixed stations and analysed for TA, pH, and DIC. During the last half  
 276 of the ATL2MED demonstration experiment, this routine was hampered due to COVID-19 restrictions, thus,  
 277 between March and July 2020, there were less discrete carbon samples for comparison with fixed station  $pCO_2$ .  
 278 Furthermore, there was minor variability in sampling frequency with regards to the fixed station  $pCO_2$   
 279 measurements and in the pair of measured variables used for  $pCO_2$  calculation (TA-pH or DIC-TA) between the  
 280 different fixed ocean stations (see Table S2 and S4). During the ATL2MED demonstration experiment, DIC, TA,  
 281 and pH were analysed according to SOP 2, 3b, and 6b, respectively (Dickson et al., 2007) with some minor local  
 282 variations (Table S4). Certified Reference Material (CRM) and TRIS provided by Prof. A. Dickson (Scripps,  
 283 USDC, USA) were used to determine the accuracy.  $pCO_2$  was calculated using the speciation software CO2SYS  
 284 (Pelletier et al., 2007), with the discrete carbon pairs TA-pH or DIC-TA as input variables. In the computation, the  
 285 carbonate system constants from Lueker et al. (2000), the  $HSO_4^-$  constant from Dickson (1990), the total borate-  
 286 salinity relationship of Lee et al. (2010), and the hydrogen fluoride constant  $K_F$  from Perez and Fraga (1987) were  
 287 used. The uncertainties connected to this calculation ranged from 1.82% when using TA-pH as input variables to  
 288 2.65% when DIC-TA were the input variables (Orr et al., 2018). Based on this, no adjustments were performed  
 289 for the fixed station  $pCO_2$  data when the deviation from  $pCO_2$  calculated from discrete carbon data were less than  
 290  $7.5 \mu atm$  and  $10 \mu atm$  for the discrete carbon pairs TA-pH and DIC-TA, respectively. Uncertainty thresholds were  
 291 set based on measurement uncertainties at each facility and temperature and  $pCO_2$  in the vicinity of the fixed  
 292 stations.

293

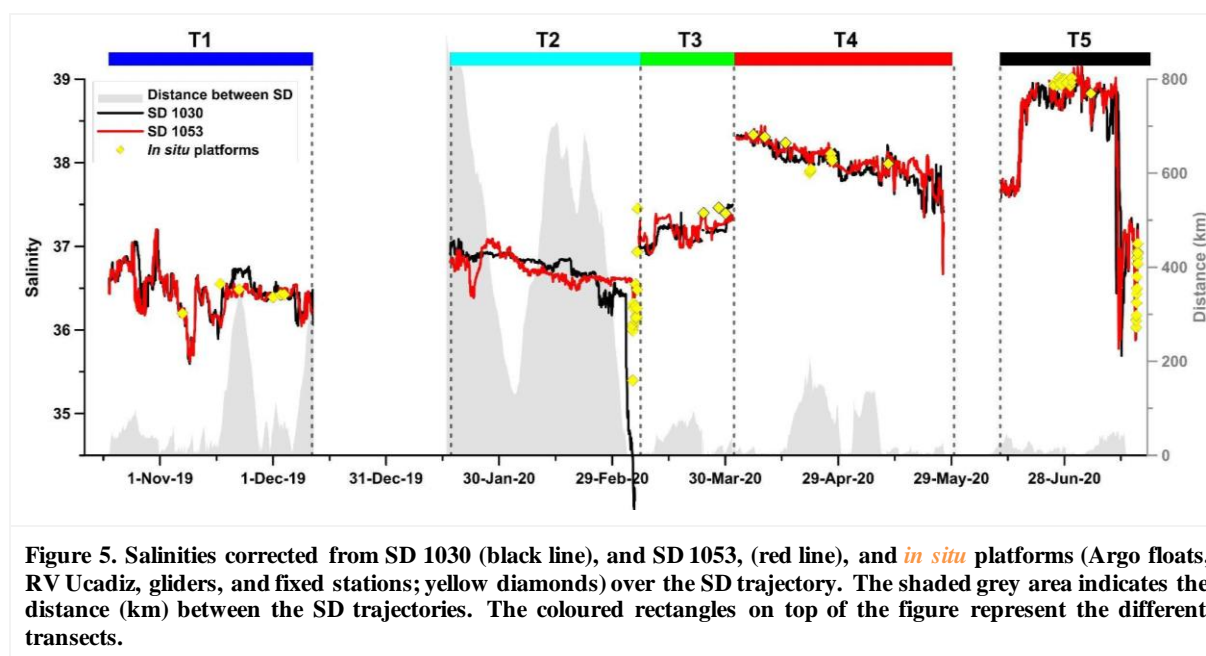
### 294 3.3.2 Correction of SD CO<sub>2</sub> data

295 The general accuracy of the ASVCO<sub>2</sub> system attached to the SD 1030 was checked by PMEL prior to deployment  
 296 by comparing the results with ESRL CO<sub>2</sub> standards traceable to WMO standards (Sutton et al., 2014). For this test,  
 297 typically 6 standard gases were used. On the return of the ASVCO<sub>2</sub> system to PMEL, it was discovered that the  
 298 span gas was adjusted too low to completely flush the detector and that this had been so during the whole  
 299 ATL2MED demonstration experiment. Thus, the LI-COR had to be recalibrated at the PMEL lab and this implied  
 300 that the onboard gas spanning was bypassed, and new calibration coefficients were developed. Furthermore, the  
 301 pre-mission test data from the PMEL lab were reprocessed using the new calibration coefficients. Based on the  
 302 reported issues with the ASVCO<sub>2</sub> instrument, the accuracy of the CO<sub>2</sub> measurements is estimated to be < 5 µatm.  
 303

## 304 4 Results and discussion

### 305 4.1 Salinity

306



307

308 The salinity correction was based on the significant linear correlation (Fig. 3) observed across the different  
 309 periods (Table 2). The periods characterised by small differences in salinity (<0.1) were not corrected. In general,  
 310 the corrected salinity for both SDs showed similar values (Fig. 5), and the major differences between the two SDs  
 311 were mainly due to their temporal and spatial distance. Overall, the correction was largest for SD 1053 (see RMSE  
 312 values in Table 2). To validate the salinity corrected data a comparison with different observing systems was done.

313 For SD1030, the corrected salinity data showed a slight overestimation of salinity, while the raw salinity data  
 314 showed an underestimation. The SD 1030 salinity highlights good agreement in T1 with respect to the SD 1053  
 315 (Fig. 5), the average difference was less than 0.05, the highest difference between Argo float data and corrected  
 316 salinity data observed on 17 November 2019 was ~0.15. In T2, the comparison can only be made for SD 1030  
 317 with only one Argo float profile.

318 Between T2 and T3 a drop in salinity was observed when the SDs crossed the ETNA area, where the salinity  
 319 exhibits a strong variability (Reverdin et al., 2007), triggered by freshwater flux and eddy transport (Gordon and  
 320 Giulivi, 2014). This salinity drop was also observed in the climatological data (Fig. 2).

321 The salinity in T2 (SD 1030) only slightly differed ( $\Delta S \sim 0.05$ ) with respect to the model and values were in  
 322 agreement with the observations of the Argo floats during the crossing of the Gibraltar strait. In T3 a significant  
 323 difference was observed between model and observation (RMSE = 0.906; Table 2), while T4 was in line with the  
 324 climatology as well as the fixed stations. In T5, the RMSE was 0.279 (Table 2), in the southern Adriatic, the SDs

325 spent four days sampling the area, which allowed a robust comparison between data from the E2M3A fixed ocean  
326 station and the glider measurements. The comparison showed a very good agreement between the observations,  
327 which had almost the same salinity. In the northern Adriatic (T5), the comparison with *in situ* data showed the  
328 highest differences with respect to the other *in situ* platforms comparison. However, the comparison with the fixed  
329 stations (MIRAMARE and PALOMA) showed the same temporal changes with an average difference between  
330 the SDs and the MIRAMARE fixed ocean station of ~0.3.

331 Regarding SD 1053, the comparison with the different fixed ocean stations shows that the corrected salinity  
332 in T2, T3, T4 and T5 are consistent with the values measured at the stations (Argo float, glider, buoy, and RV  
333 Ucadiz), the differences being mainly due to the distance between the different observatories and to the natural  
334 variability of the areas. Also, the corrected data fit well with climatological values and *in situ* platforms.  
335 Considering that during T1 the SDs raw data showed a smaller deviation from the Argo float data, the salinity  
336 correction was applied after this transect (*i.e.*, from the start of T2).

## 337 4.2 Dissolved oxygen

338 For dissolved oxygen concentration, it would have been preferable to be able to compare the SD data to discrete  
339 data. However, over the period of the ATL2MED demonstration experiment, no discrete dissolved oxygen  
340 measurements were available due to COVID-19 restrictions. The corrected oxygen measurements (Fig. 6a)  
341 spanned from 170  $\mu\text{mol/kg}$  to 270  $\mu\text{mol/kg}$  highlighting the highest concentrations during spring 2020. Time series  
342 of percent dissolved oxygen saturation did not show any significant trend (Fig. 6b). Oversaturation was observed  
343 at the end of October 2019 (~115%) and at the beginning of March 2020 (~105%), while strong undersaturation  
344 was observed at 1-2 of April 2020 (~95%) and 8-11 July 2020 (~92%).

345 Furthermore, we evaluated the change in dissolved oxygen measured by the two SDs in two different  
346 geographical areas (the Canary Islands area and the Balearic basin), where dissolved oxygen showed  
347 oversaturation (Fig. 7) and undersaturation (Fig. 8). In the first region, we made use of Chl-a data and temperature,  
348 while in the second region, temperature was used to evaluate the representativeness of the correction with respect  
349 to ecosystem dynamics. *The optical sensors on the SDs and thus, the Chl-a measurements, were strongly affected  
350 by biofouling for most of the demonstration experiment, which is why we do not use these measurements in this  
351 work. However, during the 10 first days in October 2019, the Chl-a data acquired by the SDs seemed to produce  
352 reasonable values in accordance with Delory et al. (2018), who found that for new sensors the increase in  
353 biofouling needs weeks to become significant. We refer to these Chl-a data, collected by the SDs in the transect  
354 T1, when explaining the dissolved oxygen oversaturation episode off the Canary Islands.*

355 The oxygen saturation concentration can be expressed as a function of salinity and temperature, in terms of  
356 solubility (Garcia and Gordon, 1992). The gas concentration in sea water depends on thermohaline characteristics  
357 and biological activity. The solubility of oxygen decreases with increasing temperature and salinity, showing a  
358 strong correlation. In the ocean, dissolved oxygen saturation lower than 100% can be observed during the cold  
359 seasons while in the warm season oxygen saturation is higher than 100%, inversely to the dissolved oxygen  
360 concentrations (*i.e.*, high concentrations during cold season and low in the warm season). This is because heating  
361 and cooling are generally faster than outgassing, except for episodes of high wind speeds which intensifies the air-  
362 sea gas exchange (Ulses et al., 2021). Furthermore, dissolved oxygen concentration is affected by primary  
363 production and respiration.

364

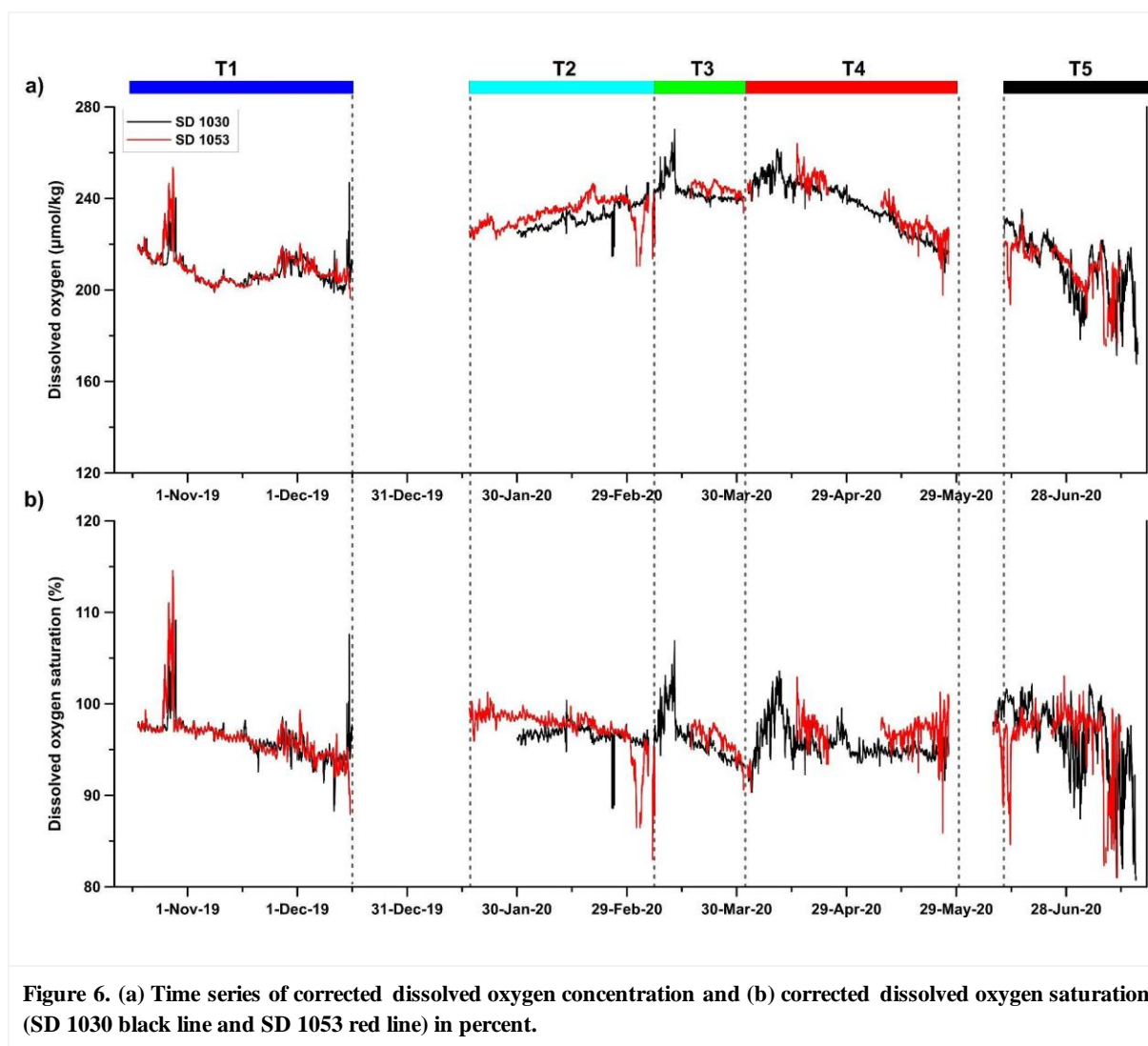
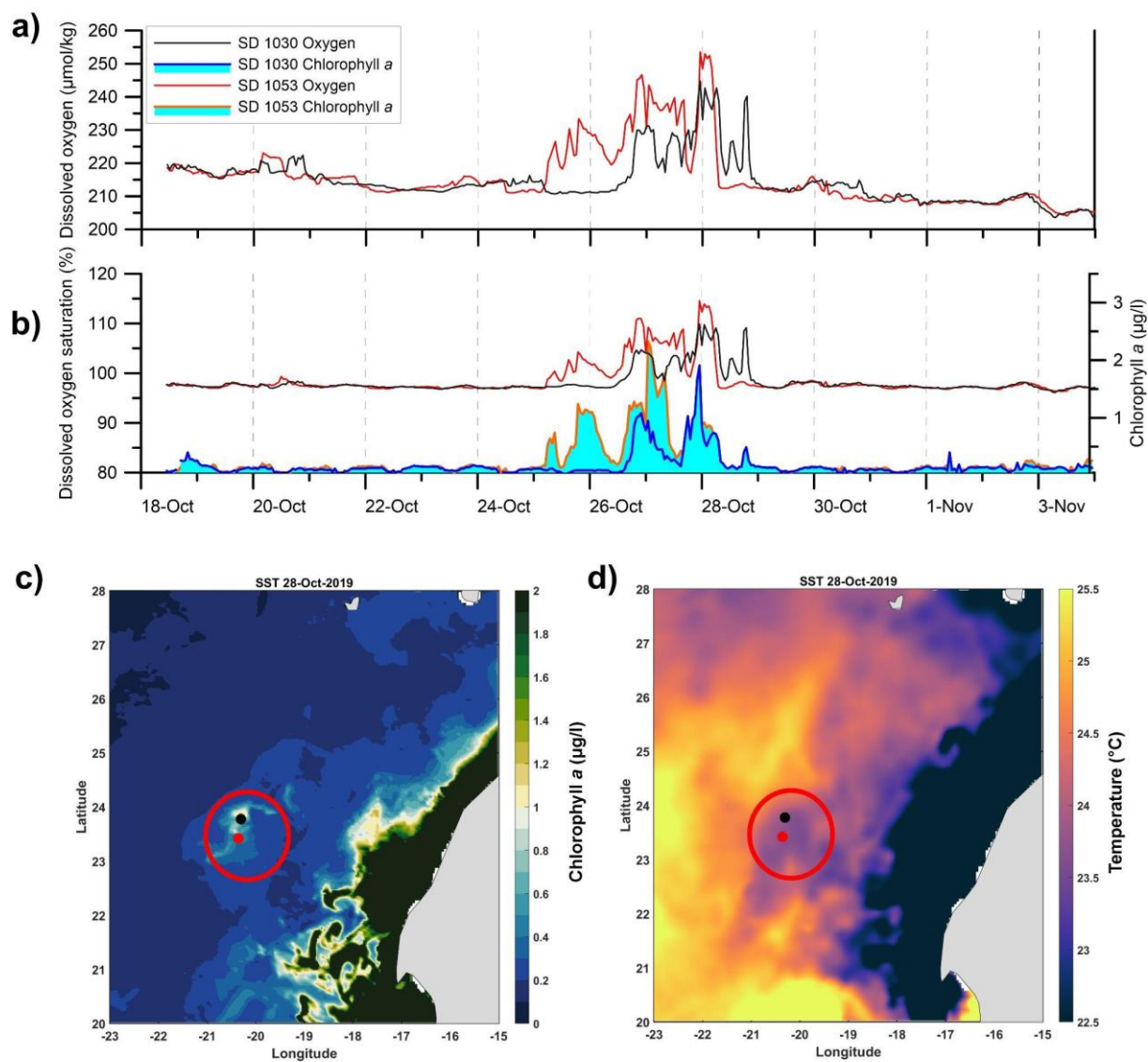


**Figure 6. (a) Time series of corrected dissolved oxygen concentration and (b) corrected dissolved oxygen saturation (SD 1030 black line and SD 1053 red line) in percent.**

365  
366  
367  
368  
369  
370  
371  
372  
373

Between October 25 and 29, the dissolved oxygen concentration and saturation were high around the Canary Islands ( $>240 \mu\text{mol/kg}$  and  $>110\%$ ; Fig. 7a and b). During the same period high concentrations of Chl-a were measured by SDs ( $\sim 2 \mu\text{g/l}$ , Fig. 7b, blue and orange line). The area with high Chl-a concentrations off the Canary Islands was visible on the satellite images of sea surface Chl-a concentration (Fig. 7c) and at the same time low sea surface temperature was observed (Fig. 7d). High Chl-a concentrations and low temperatures identify a mesoscale structure that has moved away from the African shelf. Considering that the latter is a very productive area due to the permanent upwelling off NW Africa coast (Cropper et al., 2014; Fischer et al., 2016), this justifies the high Chl-a concentration observed by the SDs at that time.

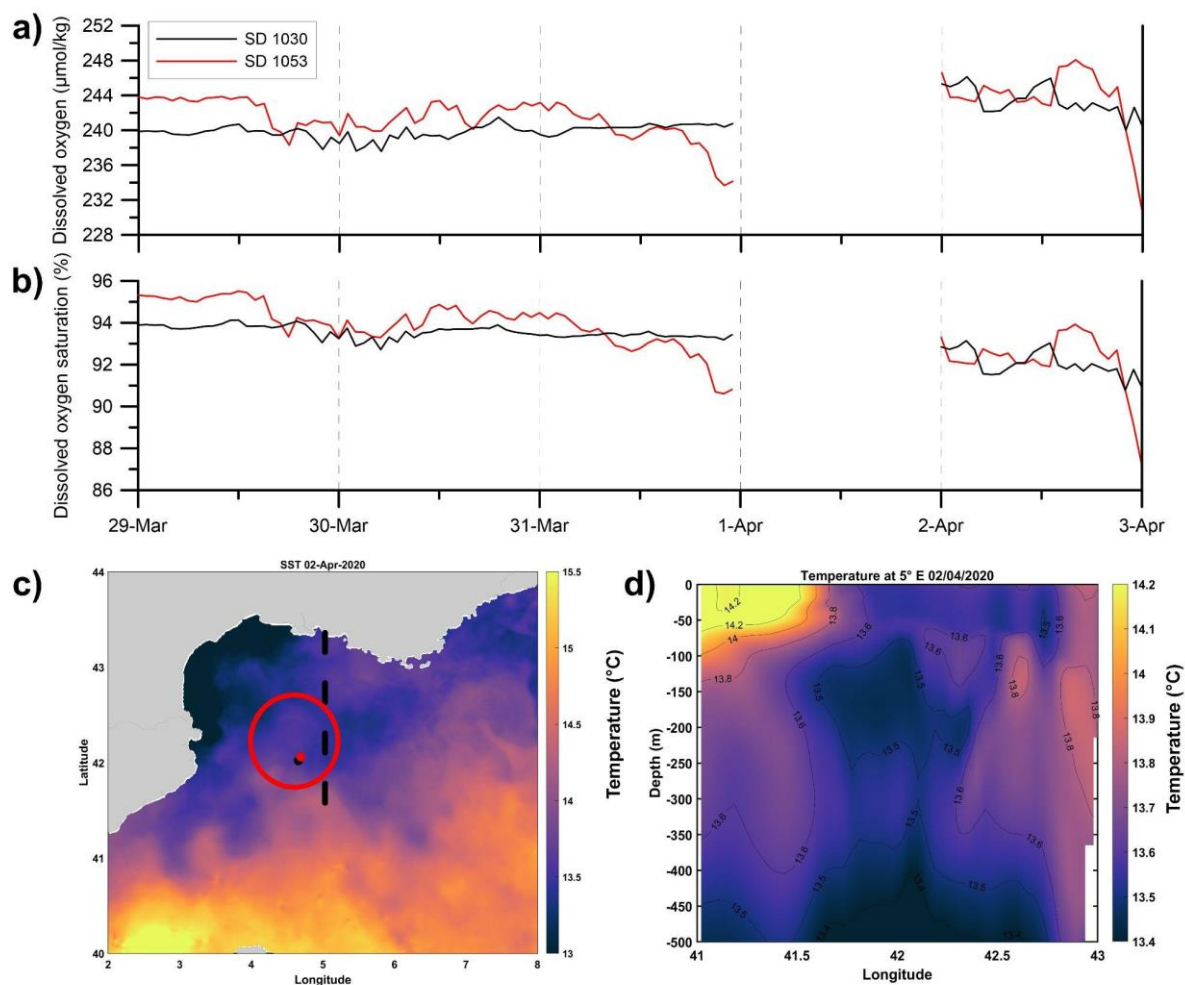




374  
 375  
 376  
 377  
 378  
 379  
 380

Figure 7. Time series of (a) dissolved oxygen concentration and (b) dissolved oxygen saturation in the Canary Islands area. Sea surface Chl-a concentration (c), and (d) sea surface temperature on 28 October 2019. The red circle highlights the position of SDs (black dot = SD1030 and red dot=SD1053).

381



382

383

**Figure 8.** Time series of (a) dissolved oxygen concentration and (b) percent dissolved oxygen saturation in the Balearic basin. (c) Sea surface temperature evolution between 31 March and 2 April 2020. The black dotted line highlights the vertical section in (d). The red circle highlights the position of SDs (black dot = SD1030 and red dot=SD1053).

386

387 Between 29 March and 3 April 2020, the SDs crossed the Balearic basin reaching the Gulf of Lion on the 1 April

388 2020, the SD 1053 measured a decrease in dissolved oxygen concentrations of about  $10 \mu\text{mol/kg}$  (Fig. 8a). This

389 behaviour was also observed in the dissolved oxygen saturation (Fig. 8b) which reached values lower than 95%.

390 The northern part of the basin was characterised by lower surface temperatures (Fig. 8c) than the southern part.

391 The vertical temperature section (Fig. 8d) highlighted the presence of upwelling of cold water to the surface justifying the lower surface temperature observed in Fig. 8c. The presence of this upwelled water caused the

392 decrease in dissolved oxygen saturation (Fig. 8b) observed by the SDs, as the upwelled water is commonly

393 characterised by low dissolved oxygen concentrations due to biological respiration (Chan et al., 2019).

395

### 396 4.3 $p\text{CO}_2$

397  $p\text{CO}_2$  (in  $\mu\text{atm}$ ) from the ASVCO2 instrument attached to the SD 1030 were calculated according to Sutton et al.

398 (2014) using T and S from the SBE37-SMP-ODO at the SD. Fig. 9a shows the uncorrected and corrected  $p\text{CO}_2$

399 acquired from the SD 1030. In Fig. 9b, the difference between corrected and uncorrected  $p\text{CO}_2$  is shown and the

400 offset increases from approximately  $1 \mu\text{atm}$  at the start of the experiment to approximately  $12 \mu\text{atm}$  at the end.

401

402

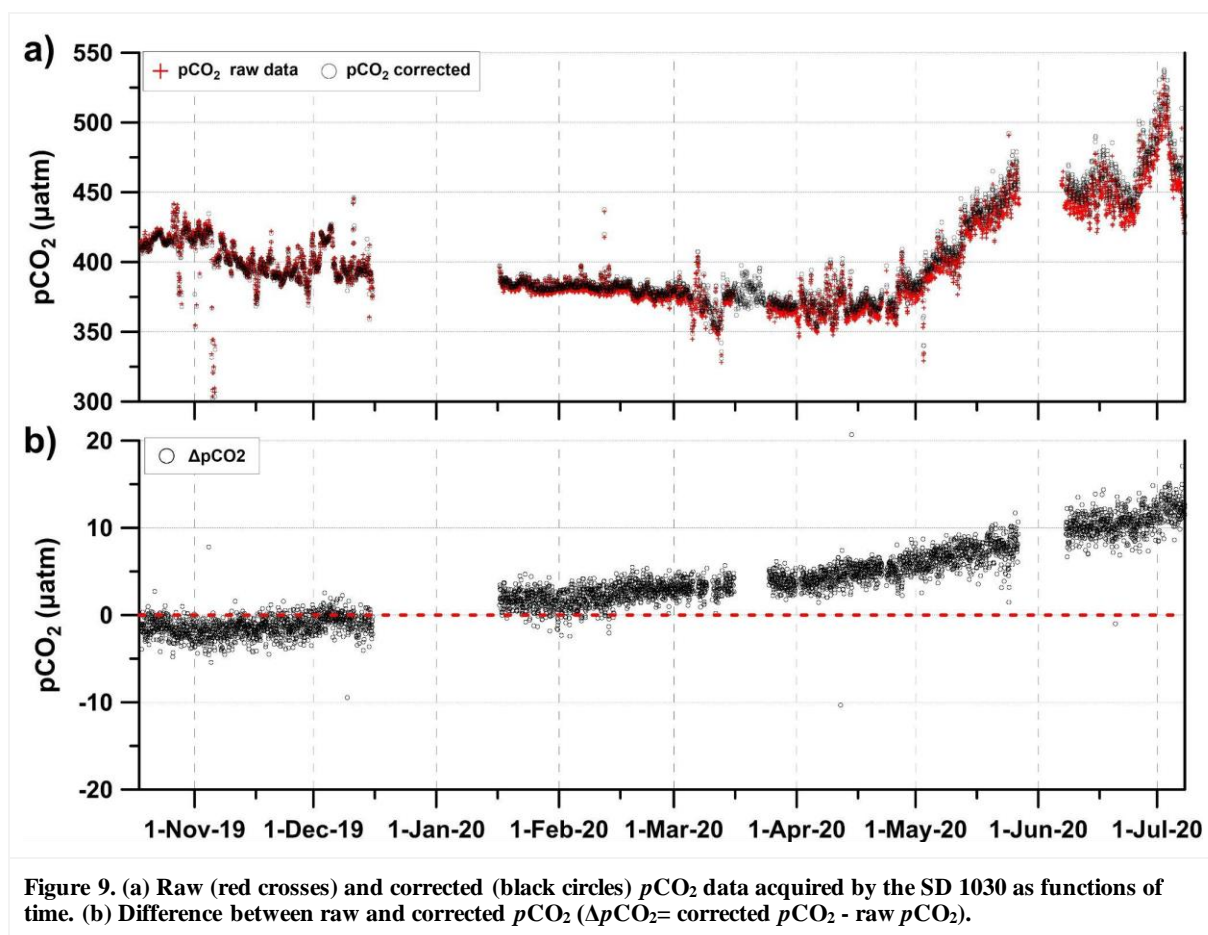
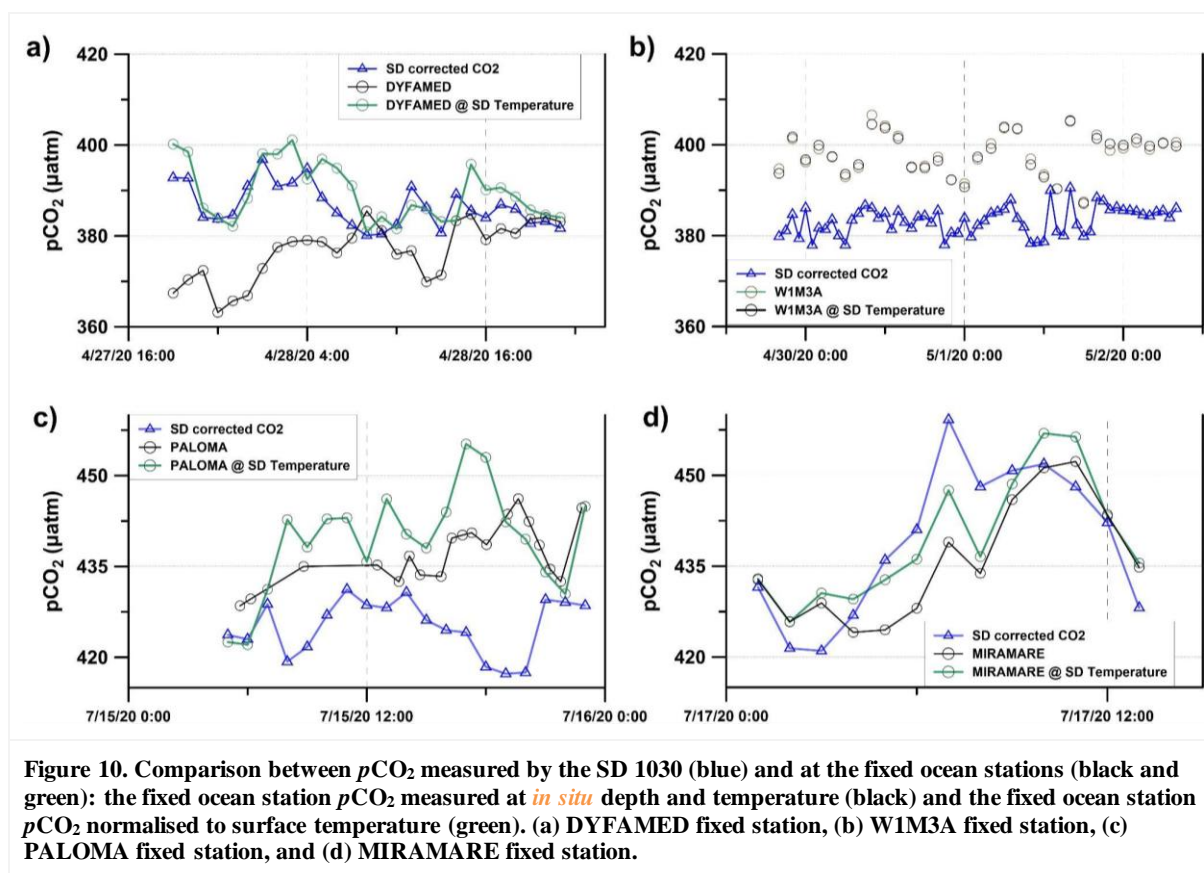


Figure 9. (a) Raw (red crosses) and corrected (black circles)  $p\text{CO}_2$  data acquired by the SD 1030 as functions of time. (b) Difference between raw and corrected  $p\text{CO}_2$  ( $\Delta p\text{CO}_2 = \text{corrected } p\text{CO}_2 - \text{raw } p\text{CO}_2$ ).

403  
 404 The  $p\text{CO}_2$  sensors at the different fixed stations were deployed at depths between 2 to 10 m while the SD measured  
 405 at 0.5 m depth. To be able to compare  $p\text{CO}_2$  measurements from the different depths, the station  $p\text{CO}_2$  data were  
 406 normalised to surface temperature by using the relationship of Takahashi et al. (1993):  $p\text{CO}_2(1) =$   
 407  $p\text{CO}_2(2) \exp^{0.0423 (T_1 - T_2)}$  (5)  
 408 where T is temperature and 1 and 2 refer to the measurements at 0.5 m depth of the SD and at the measurement  
 409 depth of each local station, respectively. Furthermore, the  $p\text{CO}_2$  measurements acquired by the SD 1030 were  
 410 compared to the corrected  $p\text{CO}_2$ , surface temperature normalised, from the fixed ocean stations (Fig. 10 and Table  
 411 3). The difference varied between -0.5 and -16.9 μatm. The largest difference occurred in the eastern Atlantic,  
 412 where calculated  $p\text{CO}_2$  from discrete DIC and TA were compared to the SD 1030  $p\text{CO}_2$  data. Part of this deviation  
 413 is likely attributed to calculation errors which is estimated to be about 10 μatm when errors in both DIC, TA, and  
 414 the carbon constants are included (Orr et al., 2018). The smallest difference between the SD 1030  $p\text{CO}_2$  and the  
 415  $p\text{CO}_2$  acquired from the fixed stations and normalised to surface temperature are seen at DYFAMED (using DIC  
 416 and TA as input; Table S4) toward the end of April 2020 (-2.9 μatm) and at MIRAMARE (using pH and TA as  
 417 input variables; Table S4) in mid July 2020 (-0.5 μatm). The larger discrepancy at WIM3A and PALOMA might  
 418 be attributed to processes which are not taken into account by temperature normalising, e.g., spatial gradients due  
 419 to primary production/remineralisation, which would decrease/increase the  $p\text{CO}_2$ . However, it is difficult to  
 420 estimate the impact of these processes.  
 421



422

423

Table 3. Comparison between  $p\text{CO}_2$  measurements at SD 1030 and the fixed ocean stations.

Station/ platform	Measurements	Date	Deviation between $p\text{CO}_2$ at SD 1030 and $p\text{CO}_2$ at fixed station normalised to SST ( $\mu\text{atm}$ )
RV Meteor	Discrete DIC and TA samples @ 5 m	30 Nov 2019	-16.9 $\mu\text{atm}$
DYFAMED	$p\text{CO}_2$ sensor @ 10 m	27-28 Apr 2020	-2.9 $\mu\text{atm}$
W1M3A	$p\text{CO}_2$ sensor @ 6 m	28 Apr - 2 May 2020	-14.2 $\mu\text{atm}$
PALOMA	$p\text{CO}_2$ sensor @ 3 m	15 July 2020	-14.7 $\mu\text{atm}$
MIRAMARE	$p\text{CO}_2$ sensor @ 2 m	17 July 2020	-0.5 $\mu\text{atm}$

424

SST= sea surface temperature

425

## 426 5 Summary

427 The ATL2MED demonstration experiment, which lasted for 273 days, represented the first monitoring  
 428 experiments of SDs covering both the ETNA region and the Mediterranean Sea, evaluating dynamics between  
 429 fixed ocean stations within the same basin as well as comparing characteristics between basins. The experiment  
 430 covered all seasons with varying meteorological and oceanographic conditions, primary productivity, and maritime  
 431 traffic. The ATL2MED lasted longer than planned primarily due to challenges with heavy biofouling of the two  
 432 SDs, COVID-19 pandemic restrictions, low winds, and strong contrary winds.

433 A huge amount of data has been produced during the ATL2MED demonstration experiment, and the data  
 434 required quality control and assurance to a varying degree, primarily depending on how sensitive the sensors were  
 435 to biofouling. Due to the COVID-19 pandemic restrictions, there was a lack of validation samples collected from



436 cruise transects, Argo floats, and fixed stations, and this has enforced a new way of thinking regarding drift  
 437 correction. The SBE salinity data acquired by the SDs have been corrected, when necessary, using model products  
 438 and the method was validated by comparing the data corrected with available *in situ* measurements. This resulted  
 439 in remarkable consistency of the salinity correction in both space and time. The data from the Aanderaa dissolved  
 440 oxygen sensors mounted on the SDs were corrected making use of in air oxygen measurements to correct the trend.  
 441 The corrected SD datasets fit well with data from fixed stations and gliders, which means that the correction  
 442 methods used are valid. The output is datasets that are available for process interpretations in future research.

443 Other SD sensors were affected by biofouling to such a degree that the datasets were unable to be corrected  
 444 given the limited samples available for validation, like *e.g.* the optical sensors for fluorescence measurements.  
 445 Some recommendations related to this issue are presented in the next section.

446 The ATL2MED demonstration experiment is an example of how ASV can be used to perform multi-variable  
 447 and high-resolution sampling from areas which are not easily accessible, *e.g.* due to remote location, limited  
 448 shiptime availability, or COVID-19 restrictions. The SDs are environmentally friendly platforms, and they,  
 449 together with other ASV, are useful as a complement in the validation of fixed ocean stations. However, the  
 450 experiment clearly shows some of the challenges faced when this type of surface vehicle is part of long-term  
 451 missions.

452

## 453 6 Experiences and recommendations

454 Our experiences and recommendations from the ATL2MED demonstration experiment can be summarised in the  
 455 following bullet points, which are explained in more detail at the end of this paragraph:

456 We experienced that

- 457 - the SD sensors were exposed to severe biofouling
- 458 - a substantially amount of effort was required to correct the SD datasets
- 459 - some of the SD sensors were mounted in an unfavourable way
- 460 - the COVID-19 pandemic limited the access to ship time and thus also collection of discrete validation  
 461 samples

462 We recommend to:

- 463 - ensure a maintenance and cleaning frequency of the SD sensors and hull which is adapted to the local  
 464 environment
- 465 - use biolimiting equipment at the SDs
- 466 - implement an automatic in air calibration procedure for the SD oxygen measurements,
- 467 - ensure that the SD sensors are mounted in such a way that they are exposed to open waters
- 468 - ensure that a sufficient amount of independent measurements (*e.g.*, salinity, dissolved oxygen, carbonate  
 469 system, Chl-a) are collected in vicinity of the SD trajectories in order to validate the SD sensors

470 In general, the use of SDs requires a severe amount of effort into securing that the data are of scientifically usable  
 471 quality. More specifically, the sensors installed on the SDs always remain in the surface layer and are exposed for  
 472 biofouling, which can be particularly impacting in relatively warm waters of the Mediterranean Sea, and not only  
 473 during summer. For future experiment, a maintenance and sensor cleaning frequency depending on the area should  
 474 be implemented. In situations where this is not possible, biolimiting equipment should be used, like UV systems  
 475 powered by the solar panels and wipers which regularly clean the optical sensors. Furthermore, regular cleaning  
 476 of the hull will also ensure the necessary manoeuvrability and navigation precision. Experiences from the  
 477 ATL2MED demonstration experiment showed that the RBR (<https://rbr-global.com/>) sensor package used on the  
 478 SDs had serious issues regarding the biofouling effect. After 9 months in sea, this is somewhat expected. However,  
 479 the SBE37 sensors seem to be more reliable and robust regarding biofouling, but a regular sensor cleaning  
 480 procedure is necessary using special devices or human interventions during the SD deployment. Regarding  
 481 correction of dissolved oxygen, it is advised to facilitate an in-air calibration like the one used for Argo floats. This  
 482 would require some reorganisation of the sensors; however, it will be easier to correct for drift of the oxygen  
 483 sensor. It is also advised to look into the location of the SD sensors. For instance, the RBR sensor on the SD 1053  
 484 measured significantly lower dissolved oxygen concentration compared to the SBE. One possible explanation for



485 this could be that the RBR sensor was mounted inside the ship keel where dead water could accelerate the sensor  
486 fouling. It must be ensured that the SD sensors are mounted correctly to sample open water.

487 The ATL2MED demonstration experiment suffered from a lack of discrete samples for validation. Thus,  
488 future experiments should be organised in such a way that discrete samples for salinity, dissolved oxygen, carbon,  
489 and Chl-a are collected at a reasonable frequency, which will ease the validation of the SD data set quality  
490 tremendously. Finally, the suitability of SDs as tool to validate other types of measuring devices (*e.g.*, fixed ocean  
491 stations, mobile platforms or ships) strongly depends on various conditions such as distance from the platforms,  
492 depth of fixed station measurements, environmental conditions and status of the sensors. All these factors need to  
493 be carefully considered to ensure the best possible data set for such a validation.

494

495 **Data availability.** Data described in this work is available from different sources, see Table S6 in the  
496 Supplementary Material.

497

498 **Supplement.** The supplementary material is available at the end of this manuscript.

499

500 **Author contribution.** RM, ...

501 **Competing interests.** The contact author declares that none of the authors has any competing interests.

502

### 503 **Acknowledgement**

504 The ATL2MED experiment has received generous funding from the US company PEAK 6 Invest and invaluable  
505 support regarding coordination, operation, and data deliverance from Sairdrone Inc.. Furthermore, funding has  
506 been provided by GEOMAR Helmholtz Centre for Ocean Research (GEOMAR), Integrated Carbon Observation  
507 System - Ocean Thematic Centre (ICOS-OTC), the French National Centre for Scientific Research (CNRS),  
508 Oceanography Laboratory of Villefranche (LOV), the Oceanic Platform of the Canary Islands (PLOCAN), Ocean  
509 Science Centre Mindelo (OSCM), the Hydrographic Institute of Portugal (IH), Balearic Islands Coastal Observing  
510 and Forecasting System (SOCIB), Italian National Institute of Oceanography and Applied Geophysics (OGS),  
511 Helmholtz Zentrum Geesthacht (HZG), Centre Scientifique de Monaco (CSM), National Research Council-  
512 Institute of Marine Sciences (CNR-ISMAR), and National Research Council - Institute for the study of Anthropic  
513 Impact and Sustainability in the Marine Environment (CNR-IAS). We thank the OGS engineers Paolo Mansutti  
514 and Giuseppe Siena for the assistance during the final recovery of the SDs, and Piero Zuppelli, Riccardo Gerin,  
515 Antonio Bussani and Massimo Pacciaroni for piloting the OGS glider. Furthermore, we thank Björn Fiedeler and  
516 Benjamin Pfeil for initialising the demonstration experiment and for executing the first phase of the experiment.  
517 Finally, we thank Adrienne Sutton and Stacy Manner for invaluable help with correcting the ASVCO<sub>2</sub> *p*CO<sub>2</sub> data.  
518

### 519 **References**

- 520 Bittig, H. C., Körtzinger, A., Neill, C., van Ooijen, E., Plant, J. N., Hahn, J., Johnson, K. S., Jang, B., and Emerson,  
521 S. R.: Oxygen optode sensors: principle, characterization, calibration, and application in the ocean, *Front. Mar.*  
522 *Sci.*, 4, 429, <https://doi.org/10.3389/fmars.2017.00429>, 2018.
- 523 Bosse, A., Testor, P., Mortier, L., Prieur, L., Taillandier, V., D'Ortenzio, F., and Coppola, L.: Spreading of  
524 Levantine Intermediate Waters by submesoscale coherent vortices in the northwestern Mediterranean Sea as  
525 observed with gliders, *J. Geophys. Res-Oceans*, 120(3), 1599-1622, <https://doi.org/10.1002/2014JC010263>,  
526 2015.

- 527 Bozzano, R., Pensieri, S., Pensieri, L., Cardin, V., Brunetti, F., Bensi, M., Petihakis, G., Tsagaraki, T. M., Ntoumas,  
 528 M., Podaras, D., and Perivoliotis, L.: The M3A network of open ocean observatories in the Mediterranean Sea,  
 529 in: 2013 MTS/IEEE OCEANS-Bergen, IEEE, Bergen, Norway, 10-14 June 2013, 1-10, 2013.
- 530 Bozzano, R. and Pensieri, S.: W1M3A fixed station data collected as part of the ATL2MED demonstration  
 531 experiment 2019-2020 [Data set], <https://hdl.handle.net/11676/Z9bGSnVObyglR0o8zcvmIXBz>, 2024.
- 532 Buongiorno Nardelli, B., Tronconi, C., Pisano, A., and Santoleri, R.: High and Ultra -High resolution processing  
 533 of satellite Sea Surface Temperature data over Southern European Seas in the framework of MyOcean project,  
 534 Copernicus Monitoring Environment Marine Service (CMEMS) [Data set], <https://doi.org/10.48670/moi-00172>, 2022.
- 535 Canepa, E., Pensieri, S., Bozzano, R., Faimali, M., Traverso, P., and Cavaleri, L.: The ODAS Italia 1 buoy: More  
 536 than forty years of activity in the Ligurian Sea, *Progr. Oceanogr.*, 135, 48-63,  
 537 <https://doi.org/10.1016/j.pocean.2015.04.005>, 2015.
- 538 Cantoni, C., Luchetta, A., Celio, M., Cozzi, S., Raicich, F., and Catalano, G.: Carbonate system variability in the  
 539 gulf of Trieste (north Adriatic Sea), *Estuar. Coast. Shelf. S.*, 115, 51-62,  
 540 <https://doi.org/10.1016/j.ecss.2012.07.006>, 2012.
- 541 Cantoni, C. and Luchetta, A.: PALOMA fixed station data collected as part of the ATL2MED demonstration  
 542 experiment 2019-2020 [Data set], <https://hdl.handle.net/11676/an-PJSKTiEVHj3H0gA8ak3IG>, 2024.
- 543 Capó, E., McWilliams, J. C., Mason, E., and Orfila, A.: Intermittent frontogenesis in the Alboran Sea. *Journal of*  
 544 *Physical Oceanography*, 51(5), 1417-1439, 2021.
- 545 Cardin, V., Ursella, L., Siena, G., Brunetti, F., Kuchler, S., and Partescano, P.: E2M3A-2017-2019-CTD-time-  
 546 series-South Adriatic [Data set],  
 547 <https://nodc.ogs.it/catalogs/doidetails;jsessionid=9D31FDE64403D9BF54F05A1F03D45FB1?0&doi=10.6092/d0d50095-bd30-4ff7-8d0a-a12121e72f78>, 2020.
- 548 Chan, F., Barth, J. A., Kroeker, K. J., Lubchenco, J., and Menge, B. A.: The dynamics and impact of ocean  
 549 acidification and hypoxia. *Oceanography*, 32(3), 62-71, 2019.
- 550 Civitarese G., Gačić M., Batistić M., Bensi M., Cardin V., Dulčić J., Garić R., Menna M.. The BIOS mechanism:  
 551 history, theory, implications. *Progress in Oceanography*, 103056. 2023.
- 552 Clayton, T. D. and Byrne, R. H.: Spectrophotometric sea water pH measurements: total hydrogen ion concentration  
 553 scale calibration of *m*-creosol purple and at-sea results. *Deep-Sea Res.*, 40, 2115-2129, 1993.
- 554 Clementi, E., Aydogdu, A., Goglio, A. C., Pistoia, J., Escudier, R., Drudi, M., Grandi, A., Mariani, A., Lyubartsev,  
 555 V., Lecci, R., Cretí, S., Coppini, G., Masina, S., and Pinardi, N.: Mediterranean Sea Physical Analysis and  
 556 Forecast (CMEMS MED-Currents, EAS6 system) (Version 1), Copernicus Monitoring Environment Marine  
 557 Service (CMEMS) [Data set],  
 558 [https://doi.org/10.25423/CMCC/MEDSEA\\_ANALYSISFORECAST\\_PHY\\_006\\_013\\_EAS7](https://doi.org/10.25423/CMCC/MEDSEA_ANALYSISFORECAST_PHY_006_013_EAS7), 2021.
- 559 Coppola, L., Raimbault, P., Mortier, L., and Testor, P.: Monitoring the environment in the northwestern  
 560 Mediterranean Sea, *Eos*, 100, <https://doi.org/10.1029/2019EO125951>, 2019.
- 561 Coppola, L., Diamond, R. E., Carval, T., Irisson J. O., and Desnos, C.: Dyfamed observatory data, SEANOE [Data  
 562 set], <https://doi.org/10.17882/43749>, 2023.
- 563 Cropper, T. E., Hanna, E., and Bigg, G. R.: Spatial and temporal seasonal trends in coastal upwelling off Northwest  
 564 Africa, 1981-2012, *Deep-Sea Res. Pt. I*, 86, 94-111, <https://doi.org/10.1016/j.dsr.2014.01.007>, 2014.
- 565 Delauney, L., Compère, C., and Lehaitre, M.: Biofouling protection for marine environmental sensors, *Ocean Sci.*,  
 566 6, 503-511, <https://doi.org/10.5194/os-6-503-2010>, 2010.
- 567 Delory, E., and Jay P., (Eds.): Challenges and Innovations in Ocean *In Situ* Sensors: Measuring Inner Ocean  
 568 Processes and Health in the Digital Age. Elsevier, 408 pp, ISBN: 9780128098868, 2018.
- 569 Dickson, A. G.: Standard potential of the reaction:  $\text{AgCl}(s) + \frac{1}{2}\text{H}_2(g) = \text{Ag}(s) + \text{HCl}(aq)$ , and the standard acidity  
 570 constant of the ion  $\text{HSO}_4^-$  in synthetic sea water from 273.15 to 318.15 K, *J. Chem. Thermodyn.*, 22, 113-  
 571 127, [https://doi.org/10.1016/0198-0149\(90\)90004-F](https://doi.org/10.1016/0198-0149(90)90004-F), 1990.
- 572 Dickson, A. G. and Goyet, C.: Handbook of methods for the analysis of the various parameters of the carbon  
 573 dioxide system in sea water. Version 2, Oak Ridge National Lab. (ORNL), <https://doi.org/10.2172/10107773>,  
 574 1994.
- 575 Dickson, A. G., Sabine, C. L., and Christian, J. R. (Eds): Guide to best practices for ocean CO2 measurements,  
 576 PICES Special Publication 3, North Pacific Marine Science Organization Sidney, British Columbia, 191,  
 577 <https://doi.org/10.25607/OBP-1342>, 2007.

- 580 Edmond, J. M. . High precision determination of titration alkalinity and total carbon dioxide content of sea water  
581 by potentiometric titration. In *Deep Sea Research and Oceanographic Abstracts* (Vol. 17, No. 4, pp. 737-750).  
582 Elsevier. 1970.
- 583 Escudier, R., Clementi, E., Cipollone, A., Pistoia, J., Drudi, M., Grandi, A., Lyubartsev, V., Lecci, R., Aydogdu,  
584 A., Delrosso, D., Omar, M., Masina, S., Coppini, G., and Pinardi, N.: A High Resolution Reanalysis for the  
585 Mediterranean Sea, *Front. Earth Sci.*, 9, <https://doi.org/10.3389/feart.2021.702285>, 2021.
- 586 Escudier, R., Clementi, E., Omar, M., Cipollone, A., Pistoia, J., Aydogdu, A., Drudi, M., Grandi, A., Lyubartsev,  
587 V., Lecci, R., Cretí, S., Masina, S., Coppini, G., and Pinardi, N.: Mediterranean Sea Physical Reanalysis  
588 (CMEMS MED-Currents) (Version 1) [Data set], Copernicus Monitoring Environment Marine Service  
589 (CMEMS), [https://doi.org/10.25423/CMCC/MEDSEA\\_MULTIYEAR\\_PHY\\_006\\_004\\_E3R1I](https://doi.org/10.25423/CMCC/MEDSEA_MULTIYEAR_PHY_006_004_E3R1I), 2020.
- 590 Fischer, G., Romero, O., Merkel, U., Donner, B., Iversen, M., Nowald, N., Ratmeyer, V., Ruhland, G., Klann, M.,  
591 and Wefer, G.: Deep ocean mass fluxes in the coastal upwelling off Mauritania from 1988 to 2012: variability  
592 on seasonal to decadal timescales, *Biogeosciences*, 13, 3071–3090, <https://doi.org/10.5194/bg-13-3071-2016>,  
593 2016.
- 594 Friederich, G. E., Brewer, P. G., Herlien, R., and Chavez, F. P.: Measurement of sea surface partial pressure of  
595 CO<sub>2</sub> from a moored buoy, *Deep-Sea Res. Pt. I*, 42, 1175–1186, [https://doi.org/10.1016/0967-0637\(95\)00044-](https://doi.org/10.1016/0967-0637(95)00044-7)  
596 7, 1995.
- 597 Gačić, M., Ursella, L., Kovačević, V., Menna, M., Malačič, V., Bensi, M., Negretti, M.-E., Cardin, V., Mirko  
598 Orlić, M., Sommeria, J., Barreto, R. V., Viboud, S., Valran, T., Petelin, B., Siena, G., and Rubino, A.: Impact  
599 of dense-water flow over a sloping bottom on open-sea circulation: laboratory experiments and an Ionian Sea  
600 (Mediterranean) example. *Ocean Sci.*, 17, 975–996, <https://doi.org/10.5194/os-17-975-2021>, 2021.
- 601 Garcia, H. E. and Gordon, L. I.: Oxygen solubility in sea water: Better fitting equations, *Limnol. Oceanogr.*, 37 (6),  
602 1307-1312, 1992.
- 603 GDAC: <ftp://ftp.ifremer.fr/argo>, last access 17-10-2023.
- 604 Gentemann, C. L., Scott, J. P., Mazzini, P. L. F., Pianca, C., Akella, S., Minnett, P. J., Comillon, P., Fox-Kemper,  
605 B., Cetinić, I., Chin, T. M., Gomez-Valdes, J., Vazquez-Cuervo, J., Tsontos, V., Yu, L., Jenkins, R., De  
606 Halleux, S., Peacock, D., and Cohen, N.: *Salidrone - Adaptively sampling the marine environment*, BAMS,  
607 <https://doi.org/10.1175/BAMS-D-19-0015.1>, 2020.
- 608 Gerin, R., Bussani, A., Kuchler, S., Martellucci, R., Pacciaroni, M., Pirro, A., Zuppelli, P., and Mauri, E: OGS  
609 GLIDER MISSION Convex20 Dataset [Data set], 2021.
- 610 Giani, M.: MIRAMARE fixed station data collected as part of the ATL2MED demonstration experiment 2019-  
611 2020 [Data set], <https://hdl.handle.net/11676/ngPlu-Q0dtDcDx2wMFTNOtnZ>, 2024.
- 612 Glueckauf, E.: The Composition of Atmospheric Air, In: *Compendium of Meteorology*, edited by: Malone, T.F.,  
613 American Meteorological Society, Boston, MA., 3-10, [https://doi.org/10.1007/978-1-940033-70-9\\_1](https://doi.org/10.1007/978-1-940033-70-9_1), 1951.
- 614 Gonzalez, A. I. and Bruno, M.: Data from RV Ucadiz, 5-6 March 2020 [Dataset], [https://fileshare.icos-](https://fileshare.icos-cp.eu/s/evLp9m685QA8ME7)  
615 [cp.eu/s/evLp9m685QA8ME7](https://fileshare.icos-cp.eu/s/evLp9m685QA8ME7), 2024.
- 616 Gordon, A. L. and Giulivi, C. F.: Ocean eddy freshwater flux convergence into the North Atlantic subtropics.  
617 *Journal of Geophysical Research: Oceans*, 119(6), 3327-3335, 2014.
- 618 Hernandez-Ayon, J. M., Belli, S. L., Zirino, A.: pH, alkalinity and total CO<sub>2</sub> in coastal seawater by potentiometric  
619 titration with a difference derivative readout, *Anal. Chim. Acta* 394, 101–108, 1999.
- 620 Johnson, K. M., Wills, K. D., Butler, D. B., Johnson, W. K. and Wong, C. S.: Coulometric total carbon dioxide  
621 analysis for marine studies, *Mar. Chem.*, 44, 167-187, 1993.
- 622 Johnson, K. S., Plant, J. N., Riser, S. C., and Gilbert, D.: Air oxygen calibration of oxygen optodes on a profiling  
623 float array, *J. Atmos. Ocean. Tech.*, 32, 2160-2172, <https://doi.org/10.1175/JTECH-D-15-0101.1>, 2015.
- 624 Kokkini, Z., Mauri, E., Gerin, R., Poulain, P.-M., Simoncelli, S., and Notarstefano, G.: On the salinity structure in  
625 the South Adriatic as derived from float and glider observations in 2013–2016, *Deep-Sea Res. Pt. II*, 171,  
626 104625, <https://doi.org/10.1016/j.dsr2.2019.07.013>, 2019.
- 627 Lee, K., Kim, T.-W., Byrne, R. H., Millero, F. J., Feely, R. A., and Liu, Y.-M.: The universal ratio of boron to  
628 chlorinity for the North Pacific and North Atlantic oceans, *Geochim. Cosmochim. Acta*, 74, 1801–1811,  
629 <https://doi.org/10.1016/j.gca.2009.12.027>, 2010.
- 630 Lueker, T. J., Dickson, A. G., and Keeling, C. D.: Ocean pCO<sub>2</sub> calculated from dissolved inorganic carbon,  
631 alkalinity, and equations for K<sub>1</sub> and K<sub>2</sub>: validation based on laboratory measurements of CO<sub>2</sub> in gas and  
632 seawater at equilibrium, *Mar. Chem.*, 70, 105-119, [https://doi.org/10.1016/S0304-4203\(00\)00022-0](https://doi.org/10.1016/S0304-4203(00)00022-0), 2000.

- 633 Lüger, H., Wallace, D. W., Körtzinger, A., & Nojiri, Y.: The pCO<sub>2</sub> variability in the midlatitude North Atlantic  
634 Ocean during a full annual cycle. *Global biogeochemical cycles*, 18(3), 2004.
- 635 Martellucci, R., Salon, S., Cossarini, G., Piermattei, V., and Marcelli, M.: Coastal phytoplankton bloom dynamics  
636 in the Tyrrhenian Sea: Advantage of integrating *in situ* observations, large-scale analysis and forecast systems,  
637 *J. Marine Syst.*, 218, 103528, <https://doi.org/10.1016/j.jmarsys.2021.103528>, 2021.
- 638 Mauri, E., Gerin, R., and Poulain, P.-M.: Measurements of water-mass properties with a glider in the South-western  
639 Adriatic Sea, *J. Oper. Oceanogr.*, 9, sup1, s3-s9, <https://doi.org/10.1080/1755876X.2015.1117766>, 2016.
- 640 Menna, M., Gačić, M., Martellucci, R., Notarstefano, G., Fedele, G., Mauri, E., Gerin, R., and Poulain, P. M.  
641 Climatic, decadal, and interannual variability in the upper layer of the Mediterranean Sea using remotely sensed  
642 and in-situ data. *Remote Sensing*, 14(6), 1322, 2022.
- 643 Menna, M., Martellucci, R., Reale, M., Cossarini, G., Salon, S., Notarstefano, G., Mauri, E., Poulain, P.-M., Gallo,  
644 A., and Solidoro, C.: Impacts of an extreme weather system on the oceanographic features of the Mediterranean  
645 Sea: the Medicane Apollo, *Sci. Rep-UK*, 13, 3870, <https://doi.org/10.1038/s41598-023-29942-w>, 2023.
- 646 Merchant, C. J., Embury, O., Bulgin, C. E., Block, T., Corlett, G. K., Fiedler, E., Good, S.A., Mittaz, J., Rayner,  
647 N.A., Berry, D., Eastwood, S., Taylor, M., Tsushima, Y., Waterfall, A., Wilson R., Donlon, C.. Satellite-based  
648 time-series of sea-surface temperature since 1981 for climate applications. *Scientific data*, 6(1), 223. 2019.
- 649 Merlivat, L., and Brault, P.: CARIOCA Buoy: Carbon Dioxide Monitor, *Sea Technol.*, 23–30, 1995.
- 650 Merlivat, L., Boutin, J., Antoine, D., Beaumont, L., Golbol, M., and Vellucci, V.: Increase of dissolved inorganic  
651 carbon and decrease in pH in near-surface waters in the Mediterranean Sea during the past two decades,  
652 *Biogeosciences*, 15, 5653–5662, <https://doi.org/10.5194/bg-15-5653-2018>, 2018.
- 653 Mihanović, H., Vilibić, I., Šepić, J., Matić, F., Ljubešić, Z., Mauri, E., Gerin, R., Notarstefano, G., and Poulain,  
654 P.-M.: Observation, Preconditioning and Recurrence of Exceptionally High Salinities in the Adriatic Sea,  
655 *Front. Mar. Sci.* 8, 834. <https://doi.org/10.3389/fmars.2021.672210>, 2021.
- 656 Neri, F., Romagnoli, T., Accoroni, S., Ubaldi, M., Garzia, A., Pizzuti, A., Campanelli, A., Grilli, F., Marini, M.,  
657 and Totti, C.: Phytoplankton communities in a coastal and offshore stations of the northern Adriatic Sea  
658 approached by network analysis and different statistical descriptors, *Estuarine, Coastal and Shelf Science*, 282,  
659 108224, 2023.
- 660 Orr, J. C., Epitalon, J.-M., Dickson, A. G., and Gattuso, J.-P.: Routine uncertainty propagation for the marine  
661 carbon dioxide system, *Mar. Chem.*, 207, 84-107, <https://doi.org/10.1016/j.marchem.2018.10.006>, 2018.
- 662 Pastor, F., Valiente, J. A., and Palau, J. L.: Sea surface temperature in the Mediterranean: Trends and spatial  
663 patterns (1982–2016). *Meteorology and climatology of the Mediterranean and Black Seas*, 297-309, 2019.
- 664 Paulsen, M. et al.: Data from RV Meteor 30 November, 2019 [Dataset], [https://fileshare.icos-](https://fileshare.icos-cp.eu/s/eyLp9m685QA8ME7)  
665 [cp.eu/s/eyLp9m685QA8ME7](https://fileshare.icos-cp.eu/s/eyLp9m685QA8ME7), 2023.
- 666 Pelletier, G., Lewis, E., and Wallace, D.: CO<sub>2</sub>SYXLS: A calculator for the CO<sub>2</sub> system in sea water for Microsoft  
667 Excel/VBA, Wash. State Dept. of Ecology/Brookhaven Nat. Lab., Olympia, WA/Upton, NY, USA, 2007.
- 668 Perez, F. F. and Fraga, F.: Association constant of fluoride and hydrogen ions in sea water, *Mar. Chem.*, 21, 161–  
669 168, [https://doi.org/10.1016/0304-4203\(87\)90036-3](https://doi.org/10.1016/0304-4203(87)90036-3), 1987.
- 670 Pinardi, N.; Cessi, P.; Borile, F.; Wolfe, C. The Mediterranean Sea Overturning Circulation. *J. Phys. Oceanogr.*  
671 2019, 49, 1699–1721. 2019.
- 672 Pirro, A., Mauri, E., Gerin, R., Martellucci, R., Zuppelli, P., and Poulain, P.-M.: New insights on the formation  
673 and breaking mechanism of convective cyclonic cones in the South Adriatic Pit during winter 2018, *J. Phys.*  
674 *Oceanogr.*, 52, 2049–2068, <https://doi.org/10.1175/JPO-D-21-0108.1>, 2022.
- 675 Poulain, P.-M., Centurioni, L., Özgökmen, T., Tarry, D., Pascual, A., Ruiz, S., Mauri, E., Menna, M., Notarstefano,  
676 G.: On the Structure and Kinematics of an Algerian Eddy in the Southwestern Mediterranean Sea. *Remote*  
677 *Sensing*, 13(15):3039. <https://doi.org/10.3390/rs13153039>, 2021.
- 678 Pranić, P., Denamie, C., Janeković, I., and Vilibić, I.: Multi-model analysis of the Adriatic dense-water dynamics,  
679 *Ocean Science*, 19(3), 649-670, 2023.
- 680 Ravaioli, M., Bergami, C., Riminucci, F., Langone, L., Cardin, V., Di Sarra, A., Aracri, S., Bastianini, M., Bensi,  
681 M., Bergamasco, A., Bommarito, C., Borghini, M., Bortoluzzi, G., Bozzano, R., Cantoni, C., Chiggiato, J.,  
682 Crisafi, E., D'Adamo, R., Durante, S., Fanara, C., Grilli, F., Lipizer, M., Marini, M., Miserochi, S., Paschini,  
683 E., Penna, P., Pensieri, S., Pugnetti, A., Raicich, F., Schroeder, K., Siena, G., Specchiulli, A., Stanghellini, G.,  
684 Vetrano, A., and Crise, A.: The RITMARE Italian Fixed-Point Observatory Network (IFON) for marine

- 685 environmental monitoring: a case study, *J. Oper. Oceanogr.*, 9: sup1, s202-s214,  
686 <https://doi.org/10.1080/1755876X.2015.1114806>, 2016.
- 687 Reverdin, G., Kestenare, E., Frankignoul, C., and Delcroix, T.: Surface salinity in the Atlantic Ocean (30 S–50 N).  
688 *Progress in Oceanography*, 73(3-4), 311-340, 2007.
- 689 Skjelvan, I., Coppola, L., Cardin, V., Juza, M., Bozzano, R., Pensieri, S., Giani, M., Siena, G., Urbini, L., Mauri,  
690 E., Martellucci, R., Cantoni, C., Luchetta, A., Izquierdo, A., Paulsen, M., and Fiedler, B.: The ATL2MED  
691 mission - experiences and lessons learnt, Technical report, ICOS-OTC, <https://doi.org/10.18160/9HK5-807K>,  
692 2021.
- 693 Skjelvan, I., Fiedler, B., and Martellucci, R.: Data from Saildrone 1030 during the ATL2MED demonstration  
694 experiment 2019-2020 [Data set], <https://hdl.handle.net/11676/QN7XZKcJ2f4kBCGxQEeDdU3P,2024a>.
- 695 Skjelvan, I., Fiedler, B., and Martellucci, R.: Data from Saildrone 1053 during the ATL2MED demonstration  
696 experiment 2019-2020 [Data set], [https://hdl.handle.net/11676/9G9rmtDvhmu-4nI4w91O11\\_g,2024b](https://hdl.handle.net/11676/9G9rmtDvhmu-4nI4w91O11_g,2024b).
- 697 Steinhoff, T., Gkritzalis, T., Lauvset S. K., Jones, S., Schuster, U., Olsen, A., Becker, M., Bozzano, R., Brunetti, F.,  
698 Cantoni, C., Cardin, V., Diverres, D., Fiedler, B., Fransson, A., Giani, M., Hartman, S., Hoppema, M.,  
699 Jeansson, E., Johannessen, T., Kitidis, V., Körtzinger, A., Landa, C., Lefèvre, N., Luchetta, A., Naudts, L.,  
700 Nightingale, P. D., Omar, A. M., Pensieri, S., Pfeil, B., Castaño-Primo, R., Rehder, G., Rutgersson, A., Sanders,  
701 R., Schewe, I., Siena, G., Skjelvan, I., Soltwedel, T., van Heuven, S., and Watson, A.: Constraining the Oceanic  
702 Uptake and Fluxes of Greenhouse Gases by Building an Ocean Network of Certified Stations: The Ocean  
703 Component of the Integrated Carbon Observation System, ICOS-Oceans, *Frontiers in Marine Science*, vol. 6,  
704 p. 544, doi:10.3389/fmars.2019.00544, 2019.
- 705 Sutton, A. J., Sabine, C. L., Maenner-Jones, S., Lawrence-Slavas, N., Meinig, C., Feely, R. A., Mathis, J. T.,  
706 Musielewicz, S., Bott, R., McLain, P. D., Fought, J., and Kozyr, A.: A high-frequency atmospheric and  
707 sea water pCO<sub>2</sub> data set from 14 open ocean sites using a moored autonomous system, *Earth Sys. Sci. Data*, 6,  
708 353–366, <https://doi.org/10.5194/essd-6-353-2014>, 2014.
- 709 Takahashi, T., Olafsson, J., Goddard, J. G., Chipman, D. W., and Sutherland, S. C.: Seasonal variation of CO<sub>2</sub> and  
710 nutrients in the high-latitude surface oceans: a comparative study, *Glob. Biogeochem. Cy.*, 7, 843-878,  
711 <https://doi.org/10.1029/93GB02263>, 1993.
- 712 Takeshita, Y., Martz, T. R., Johnson, K. S., Plant, J. N., Gilbert, D., Riser, S. C., Craig, N. Tilbrook, B. (2013). A  
713 climatology-based quality control procedure for profiling float oxygen data. *Journal of Geophysical Research:*  
714 *Oceans*, 118(10), 5640-5650.
- 715 Tanhua, T., McCurdy, A., Fischer, A., Appeltans, W., Bax, N., Currie, K., DeYoung, B., Dunn, D., Heslop, E.,  
716 Glover, L.K., Gunn, J., Hill, K., Ishii, M., Legler, D., Lindstrom, E., Miloslavich, P., Moltmann, T., Nolan, G.,  
717 Palacz, A., Simmons, S., Sloyan, B., Smith, L.M., Smith, N., Telszewski, M., Visbeck, M., and Wilkin, J.:  
718 What We Have Learned From the Framework for Ocean Observing: Evolution of the Global Ocean Observing  
719 System. *Front. Mar. Sci.* 6:471. doi: 10.3389/fmars.2019.0047, 2019.
- 720 Testor, P., Mortier, L., Coppola, L., Claustre, H., D'Ortenzio, F., Bourrin, F., Durrieu de Madron, X., and  
721 Raimbault, P., Glider MOOSE sections [data set], <https://www.seanoe.org/data/00409/52027/>, 2017.
- 722 Testor, P., de Young, B., Rudnick, D. L., Glenn, S., Hayes, D., Lee, C. M., Pattiaratchi, C., Hill, K., Heslop, E.,  
723 Turpin, V., Alenius, P., Barrera, C., Barth, J. A., Beaird, N., Bécu, G., Bosse, A., Bourrin, F., Brearley, J. A.,  
724 Chao, Y., Chen, S., Chiggiato, J., Coppola, L., Crout, R., Cummings, J., Curry, B., Curry, R., Davis, R., Desai,  
725 K., DiMarco, S., Edwards, C., Fielding, S., Fer, I., Frajka-Williams, E., Gildor, H., Goni, G., Gutierrez, D.,  
726 Haugan, P., Hebert, D., Heiderich, J., Henson, S., Heywood, K., Hogan, P., Houpert, L., Huh, S., Inall, E.,  
727 Ishii, M., Ito, S.-i., Itoh, S., Jan, S., Kaiser, J., Karstensen, J., Kirkpatrick, B., Klymak, J., Kohut, J., Krahmann,  
728 G., Krug, M., McClatchie, S., Marin, F., Mauri, E., Mehra, A., Meredith, P., Meunier, T., Miles, T., Morell, J.  
729 M., Mortier, L., Nicholson, S., O'Callaghan, J., O'Conchubhair, D., Oke, P., Pallàs-Sanz, E., Palmer, M., Park,  
730 J., Perivoliotis, L., Poulain, P.-M., Perry, R., Queste, B., Rainville, L., Rehm, E., Roughan, M., Rome, N.,  
731 Ross, T., Ruiz, S., Saba, G., Schaeffer, A., Schönau, M., Schroeder, K., Shimizu, Y., Sloyan, B. M., Smeed,  
732 D., Snowden, D., Song, Y., Swart, S., Tenreiro, M., Thompson, A., Tintore, J., Todd, R. E., Toro, C., Venables,  
733 H., Wagawa, T., Waterman, S., Watlington, R. A., and Wilson, D.: OceanGliders: A component of the  
734 integrated GOOS, *Front. Mar. Sci.*, 6, <https://doi.org/10.3389/fmars.2019.00422>, 2019.



735 Ulses, C., Estournel, C., Fourier, M., Coppola, L., Kessouri, F., Lefèvre, D., and Marsaleix, P.: Oxygen budget  
 736 of the north-western Mediterranean deep- convection region, *Biogeosciences*, 18, 937–960,  
 737 <https://doi.org/10.5194/bg-18-937-2021>, 2021.

738 Wong, A. P. S., Wijffels, S. E., Riser, S. C., Pouliquen, S., Hosoda, S., Roemmich, D., Gilson, J., Johnson, G. C.,  
 739 Martini, K., Murphy, D. J., Scanderbeg, M., Bhaskar, T. V. S. U., Buck, J. J. H., Merceur, F., Carval, T., Maze,  
 740 G., Cabanes, C., André, X., Poffa, N., Yashayaev, I., Barker, P. M., Guinehut, S., Belbéoch, M., Ignaszewski,  
 741 M., Baringer, M. O. N., Schmid, C., Lyman, J. M., McTaggart, K. E., Purkey, S. G., Zilberman, N., Alkire, M.  
 742 B., Swift, D., Owens, W. B., Jayne, S. R., Hersh, C., Robbins, P., West-Mack, D., Bahr, F., Yoshida, S., Sutton,  
 743 P. J. H., Cancouët, R., Coatanoan, C., Dobbler, D., Juan, A. G., Gourrion, J., Kolodziejczyk, N., Bernard, V.,  
 744 Bourlès, B., Claustre, H., D'Ortenzio, F., Le Reste, S., Le Traon, P. Y., Rannou, J. P., Saout-Grit, C., Speich,  
 745 S., Thierry, V., Verbrugge, N., Angel-Benavides, I. M., Klein, B., Notarstefano, G., Poulain, P. M., Véléz-  
 746 Belchí, P., Suga, T., Ando, K., Iwasaka, N., Kobayashi, T., Masuda, S., Oka, E., Sato, K., Nakamura, T., Sato,  
 747 K., Takatsuki, Y., Yoshida, T., Cowley, R., Lovell, J. L., Oke, P. R., van Wijk, E. M., Carse, F., Donnelly, M.,  
 748 Gould, W. J., Gowers, K., King, B. A., Loch, S. G., Mowat, M., Turton, J., Rama Rao, E. P., Ravichandran,  
 749 M., Freeland, H. J., Gaboury, I., Gilbert, D., Greenan, B. J. W., Ouellet, M., Ross, T., Tran, A., Dong, M., Liu,  
 750 Z., Xu, J., Kang, K. R., Jo, H. J., Kim, S. D., and Park, H. M.: Argo Data 1999–2019: Two Million  
 751 Temperature-Salinity Profiles and Subsurface Velocity Observations From a Global Array of Profiling Floats,  
 752 *Front. Mar. Sci.*, 7, 700, <https://doi.org/10.3389/fmars.2020.00700>, 2020.

753  
754  
755

## 756 Supplementary material

756  
757

758 **Table S1. Harbours and dates of SD maintenance, of which all took place in 2020.**

Drone	Place	Mindelo (CV)	Telde, Gran Canaria (ES)	Porquerolles (FR)	Imperia (IT)	Cefalù, Sicily (IT)
SD 1030			12 February	22-23 April		26 May - 6 June
SD 1053		4-14 January			7 May	26 May - 6 June

759  
760  
761

**Table S2. Instruments, sensors, accuracy, and associated measurement frequency at the different fixed ocean stations, gliders, and ship during the ATL2MED demonstration experiment.**

Instrument/ sensor	Company/ reference	Variable	Accuracy	Measurement frequency	Used by
SBE37	Sea-Bird Scientific	T Cond	0.002°C, 0.0003 S/m	10/min	DYFAMED
SBE41 (GPCTD)	Sea-Bird Scientific	T Cond	0.002°C, 0.0003 S/m	1/s	Glider MOOSE T00
SBE19	Sea-Bird Scientific.	T Cond	0.005°C, 0.0005 S/m	2/day	MIRAMARE
SBE16 plus v2	Sea-Bird Scientific	T Cond	0.005°C, 0.0005 S/m	12/day	WIM3A
SBE41 (GPCTD)	Sea-Bird Scientific	T Cond	0.002°C, 0.0003 S/m	1/s	Glider South Adriatic
SBE37-SMP-ODO	Sea-Bird Scientific	T Cond	0.002°C, 0.0003 S/m,	15/min 60/min	PALOMA, MIRAMARE

		O <sub>2</sub>	3 µmol/kg		
CARIOCA	Merlivat and Brault (1995)	pCO <sub>2</sub>	2 µatm	24/day	DYFAMED
CO <sub>2</sub> -proCV	Pro-Oceanus Systems Inc	pCO <sub>2</sub>	2 µatm	12/day 6/day 24/day	W1M3A E2M3A MIRAMARE
Contros Hydro C systems	4H-JENA engineering GmbH	pCO <sub>2</sub>	2 µatm	1/min	PALOMA
SBE21	Sea-Bird Scientific	Cond	0.001 S/m	2/min	RV Ucadiz

T= temperature; Cond=conductivity; O<sub>2</sub>=dissolved oxygen; pCO<sub>2</sub>=partial pressure of carbon dioxide.

762  
763  
764  
765

**Table S3. Instruments and sensors at the SDs from Saildrone Inc. during the ATL2MED demonstration experiment and used in this work.**

Instrument/ sensor	Company/ reference	Variable	Accuracy	Measurement frequency
SBE37-SMP-ODO (SD 1030; SD 1053)	Sea-Bird Scientific	T Cond O <sub>2</sub>	0.002°C, 0.0003 S/m, 3 µmol/kg	10/min
ASVCO2 (SD 1030)	PMEL, Sutton et al. (2014)	pCO <sub>2</sub>	2 µatm	24/day

T= temperature; Cond=conductivity; O<sub>2</sub>=dissolved oxygen; pCO<sub>2</sub>=partial pressure of carbon dioxide.

766  
767  
768  
769

**Table S4. Instruments and methods used to analyse discrete samples collected at the RV Meteor and from different fixed stations during the ATL2MED demonstration experiment.**

Instrument/ sensor	Company/ reference (SOP)	Variable	Accuracy	# measurements (depth)	Facility
Simultaneous potentiometric acid titration using a closed cell	SNAPO-CO2 prototype, Edmond (1970), Dickson and Goyet (1994)	DIC, TA	± 2 to 5 µmol/kg	1 (5 m)	DYFAMED
SOMMA	UiC (SOP 2), Johnson (1993)	DIC	2 µmol/kg	1 (5 m)	GEOMAR
VINDTA 3S/VINDTA 3C	MARIANDA (SOP 3b)	TA	3 µmol/kg	1 (5 m)	GEOMAR
Automatic potentiometric titrator	Hanna Instruments Titrator HI931	TA	± 4 µmol/kg	3 (6 m)	W1M3A
Automatic potentiometric titrator	Metrohm 685 Dosimat (Hernandez-Aylon, 1999)	TA	3 µmol/kg	5 (0.5, 3 m) <sup>1</sup>	PALOMA
Automatic potentiometric titrator	Mettler Toledo G20/SOP3b	TA	± 4 µmol/kg	10 (0.5, 2 m)	MIRAMARE
pH metre	Mettler Toledo Seven Compact	pH	± 0.001	3 (6 m)	W1M3A
Varian Cary 50 spectrophotometer	Varian, Clayton and Byrne (1993) (SOP 6b)	pH	± 0.003	5 (0.5, 3 m) <sup>2</sup>	PALOMA

Varian Cary 100 Spectrophotometer	Varian, Clayton and Byrne (1993) (SOP 6b)	pH	± 0.002	10 (0.5, 2 m)	MIRAMARE
-----------------------------------	---	----	---------	---------------	----------

770 O<sub>2</sub>=dissolved oxygen; DIC=Dissolved Inorganic Carbon; TA=Total Alkalinity.

771 <sup>1</sup> For each measurement, 2 replicate samples were collected and analysed.

772 <sup>2</sup> For each measurement, 2 replicate samples were collected and 2-3 analyses were performed at each replicate.

773 SOP=Standard Operating Procedure according to Dickson et al. (2007).

774

775 **Table S5. Temperature offsets between SD sensor (SBE37-SMP-ODO) at 0.5 m depth and fixed stations during the**  
776 **ATL2MED demonstration experiment. More details are available in Skjelvan et al. (2021).**

Fixed station/ glider	Measurement depth (m)	SD 1030 offset (°C)	SD 1053 offset (°C)
W1M3A	1	-0.006	-0.026
E2M3A	1.7	0.216	0.138
OGS ocean glider	0.5	0.063	0.063
PALOMA	0.5	0.077	0.090
PALOMA	3	-0.061	-0.046
MIRAMARE	0.5	-0.085	-0.205
MIRAMARE	2	-0.117	-0.238

777

778

779

**Table S6. Overview over where to find the data used in the current work.**

Platform	Variables used in current work	doi or pid	Reference
SD 1030	T, S, O <sub>2</sub> , pCO <sub>2</sub>	<a href="https://hdl.handle.net/11676/QN7XZKcJ2f4kBCGxQEeDdU3P">https://hdl.handle.net/11676/QN7XZKcJ2f4kBCGxQEeDdU3P</a>	Skjelvan et al.(2024a)
SD 1053	T, S, O <sub>2</sub>	<a href="https://hdl.handle.net/11676/9G9rntDvhmu-4nI4w91O11_g">https://hdl.handle.net/11676/9G9rntDvhmu-4nI4w91O11_g</a> ,	Skjelvan et al. (2024b)
RV Meteor	T, S, DIC, TA	<a href="https://filesfare.icos-cp.eu/s/eyLp9m685QA8ME7">https://filesfare.icos-cp.eu/s/eyLp9m685QA8ME7</a>	Paulsen et al. (2023)
RV Ucadiz	S	<a href="https://filesfare.icos-cp.eu/s/eyLp9m685QA8ME7">https://filesfare.icos-cp.eu/s/eyLp9m685QA8ME7</a>	Gonzalez and Bruno (2024)
DYFAMED/ BOUSSOLE fixed station	T, S, DIC, TA, pCO <sub>2</sub>	<a href="https://doi.org/10.17882/43749">https://doi.org/10.17882/43749</a>	Coppola et al., 2023
Nice - Calvi glider	S	<a href="https://www.seanoe.org/data/00409/52027/">https://www.seanoe.org/data/00409/52027/</a> , doi from the MOOSE program (glider SLOCUM Theque on MOOSE T00_43 section)	Testor et al. (2017)
W1M3A fixed station	T, S, pCO <sub>2</sub>	<a href="https://hdl.handle.net/11676/Z9bGSnVObyglR0o8zcvmlXBz">https://hdl.handle.net/11676/Z9bGSnVObyglR0o8zcvmlXBz</a>	Bozzano and Pensieri (2024)
E2M3A fixed station	T, S, pCO <sub>2</sub>	<a href="https://nodc.ogs.it/catalogs/doidetails?4&amp;doi=10.6092/d0d50095-bd30-4ff7-8d0a-a12121e72f78">https://nodc.ogs.it/catalogs/doidetails?4&amp;doi=10.6092/d0d50095-bd30-4ff7-8d0a-a12121e72f78</a>	Cardin et al. (2020)
E2M3A glider	S	<a href="https://nodc.ogs.it/catalogs/doidet">https://nodc.ogs.it/catalogs/doidet</a>	Gerin et al. (2021)

		<a href="https://doi.org/10.13120/e7277c6b-444a-4d61-8288-596af1bac3ff">ails?8&amp;doi=10.13120/e7277c6b-444a-4d61-8288-596af1bac3ff</a>	
PALOMA fixed station	T, S, pH, TA, $pCO_2$	<a href="https://hdl.handle.net/11676/and-PJSKtiEVHj3H0gA8ak3IG">https://hdl.handle.net/11676/and-PJSKtiEVHj3H0gA8ak3IG</a>	Cantoni and Luchetta (2024)
MIRAMARE fixed station	T, S, pH, TA, $pCO_2$	<a href="https://hdl.handle.net/11676/ngPlu-Q0dtDcDx2wMFTNOtnZ">https://hdl.handle.net/11676/ngPlu-Q0dtDcDx2wMFTNOtnZ</a>	Giani (2024)
Argo buoy	S	<a href="https://doi.org/10.48670/moi-00044">https://doi.org/10.48670/moi-00044</a>	Wong et al. (2020)
CMEMS	Model product  Chl-a  SST  Vertical structure of sea temperature	<a href="https://doi.org/10.25423/CMCC/MEDSEA_ANALYSISFORECAST_PHY_006_013_EAS7">https://doi.org/10.25423/CMCC/MEDSEA_ANALYSISFORECAST_PHY_006_013_EAS7</a> ;  OCEANCOLOUR_MED_BGC_L3_NRT_009_141, doi:10.48670/moi-00297;  SST_MED_SST_L4_NRT_OBSERVATIONS_010_004, doi:10.48670/moi-00172;  MEDSEA_MULTIYEAR_PHY_006_004, doi:10.25423/CMCC/MEDSEA_MULTIYEAR_PHY_006_004_E3R	Clementi et al. (2021)

780 T=temperature; S=salinity;  $O_2$ =dissolved oxygen; DIC=Dissolved Inorganic Carbon; TA=Total Alkalinity;  $pCO_2$ =partial  
781 pressure of carbon dioxide.  
782  
783  
784